FOSSEE, IIT Bombay
OpenFOAM Semester-long Internship
August 10, 2021

Large Eddy Simulation of a confined planar jet opening in a rectangular channel

Binayak Lohani
Department of Mechanical and Aerospace Engineering
Pulchowk Campus,Nepal

Abstract

The primary aim of the paper is to simulate the laminar-turbulent transition of confined planar jet opening in a rectangular channel using Large Eddy Simulation (LES), as implemented in OpenFOAM. LES is used to resolve the large eddies and model the small eddies present in the flow. The case depicts the duct flow which has multiple applications in engineering and science such as pipe flow, HVAC systems, rectangular exhaust nozzles in aircraft connecting engine and nozzle, etc. A sub-grid turbulence modelling called Smagorinsky model using Van Driest damping function is considered in the problem. Due to the increasing interest of LES to simulate the flow in research and industries, the familiarity with the usage of this method is important. Hence, it is important to study and analyze the location of fully developed turbulent flow for a given domain and collect the mature mean and statistics from the flow.

1 Introduction

Turbulent flow in a rectangular channel is a classical problem in Computational Fluid Dynamics (CFD) to investigate the turbulent characteristics in the flow. With the involvement of jet at the inlet of the channel makes this project a combination of two widely conducted LES studies lately. The flow along the length of the channel is non-homogeneous that triggers the turbulence that are anisotropic in nature. Hence, the moments generated as a result of fluctuating component of velocity changes whenever the axis of rotation and reflection. The problem is also considered as the primary or starting stage to learn the simulating techniques for LES. Turbulent eddies consists of eddies with a range of sizes and energies. The most commonly used turbulence modelling technique is RANS where every eddies in the flow are modelled. In DNS, all the eddies are resolved but is computationally very expensive. Another technique to capture the turbulent nature in the flows is LES which is gaining popularity after the increasing computational power. In LES, the large eddies in the flow are resolved whereas smaller eddies are modelled as in RANS calculation. For this, we need to have perfect temporal and spatial resolutions which meets the computational resources

available. The flow along the length of the channel is non-homogeneous due to the confined geometry that triggers the turbulence that are anisotropic in nature. Hence, the moments generated as a result of fluctuating component of velocity changes whenever the axis of rotation and reflection.

The study is conducted for a wide range of Reynolds number so that the dependence of grid resolution with changing Reynolds number is analysed carefully. Also, the standard procedure to follow while conducting such a simulation is discussed in detail. The most significant challenge while performing LES simulation is the generation of turbulent-alike inflow conditions at the inlet. And, the persistence of turbulent nature in the flow is another problem to be addressed. The Reynolds stresses terms are the important statistical parameters that needs to be collected carefully in order to compare the obtained results with the experimental results. Gohil et al. (2012) discusses that the flow structures vary significantly even at low Reynolds number in a jet flow condition. O'neill et al. (2004) studied two low-Reynolds number cases in a circular jet flow and observed transition occurred at 680-1030 Reynolds number.

A number of experimental and computational studies have been made, Lee and Moser (2015), to study the behaviour of turbulent eddies in the channel. Gohil et al. (2013), Cohen and Wygnanski (1987) studied about the instabilities occurring in the circular jet. Imparting perturbations at inlet conditions assisted for the onset of instabilities and critical Reynolds number was found at the range of 500-525. Without the perturbation the critical Reynolds number was observed at the range of 900-925 which was numerically analysed using Direct Numerical Simulation (DNS) by Gohil et al. (2012). Aspect ratio of the rectangular channel also play important role in the laminar-turbulent transition in the flow. Hanks and Ruo (1966) made a theoretical analysis upon the transition regime in the flow in rectangular confined ducts and concluded that critical Reynolds number may vary with the aspect ratio of the channel. For aspect ratio of 3.92, it theoretically analysed that the critical Reynolds number can be at Reynolds number of 2315. According to the trend observed by the authors, critical Reynolds number increases for the channel with higher aspect ratio.

2 Problem Statement

In order to study the behaviour of a confined planar jet opening in a rectangular channel, proper dimensions need to be considered to achieve the fully developed turbulent flow. The dimensions of the channel is described in table 1. The simulation method used is LES using Smagorinsky model in OpenFOAM with Van-Driest damping function. The simulation is performed for five Reynolds number ranging from 100-2400. The length of the domain is to be carefully determined so that the flow is fully turbulent and developed in temporal and spatial analysis. For this, perturbations are added at the inlet of the jet which is considered as a standard procedure for LES simulations unlike RANS simulation where the inlet velocity is constant.

Table 1: Dimensions of the channel

	Length of channel (L)	Width of channel (S)	Height of channel (W)	Height of planar jet inlet (D)
Dimensions (mm)	Variable (to be determined)	40	10	5

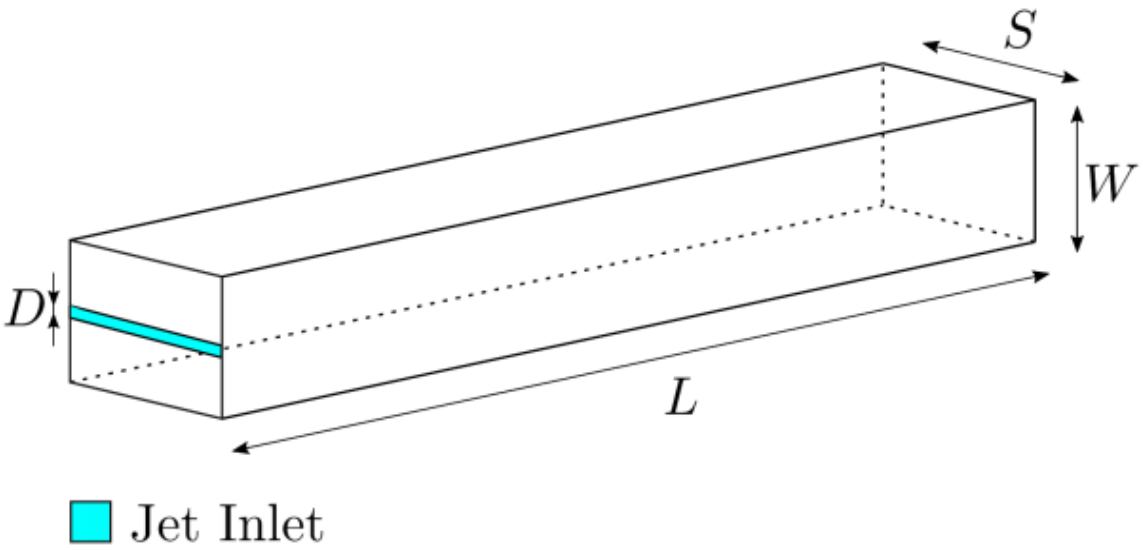

Figure 1: Geometry of the channel

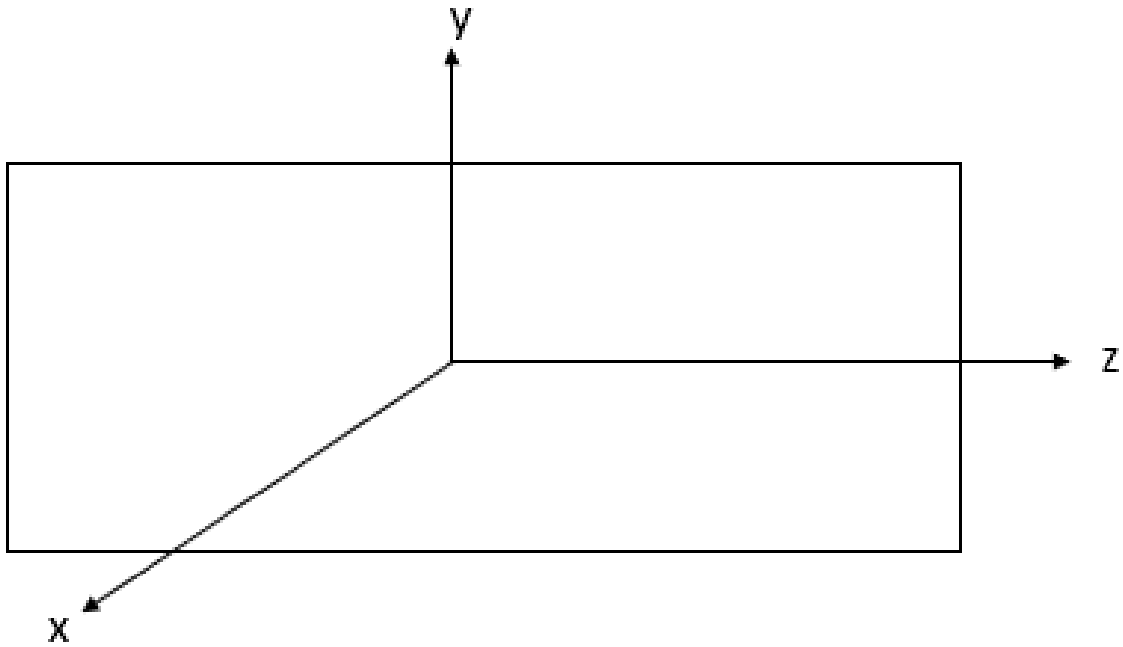

Figure 2: Cross section of the channel

The channel can be represented by the non-dimensional parameters as Y and Z as in equation (1).

$$Y = \frac{y}{D}, \qquad Z = \frac{z}{D} \tag{1}$$

The channel length varies from -1 to 1 along Y and -4 to 4 along Z direction.

3 Governing Equations and Models

In order to visualize the flow, Navier Stokes(NS) equations is considered to be the most vital part in solving the flow. Basic flows such as potential flow is generally solved analytically whereas complex flows needs to be solved computationally. For an incompressible viscous flow, mass and momentum conservation equation contributes as NS equations which in the absence of any external factors can be mathematically expressed as (2) and (3) respectively.

$$\frac{\partial u_j}{\partial x_j} = 0 \tag{2}$$

$$\frac{\partial u_i}{\partial t} + \frac{\partial \left(u_i u_j\right)}{\partial x_j} = -\frac{\partial P}{\partial x_i} + \frac{1}{Re}\frac{\partial \left(\tau_{ij}\right)}{\partial x_j} \tag{3}$$

where,

$\tau_{ij} = (1+\nu_t)/(\frac{\partial u_i}{\partial x_j}+\frac{\partial u_j}{\partial x_i})$ is the viscous stress tensor. This term is responsible for the dissipation of energy through molecular viscosity. The indices i, j =1, 2, 3 are the Einstein's notations for different directions x, y and z in the domain. The instantaneous velocity term can be represented as a sum of fluctuating and mean velocity as in equation (4).

$$u = u' + u_m \tag{4}$$

The mean velocity (u_m) can be modelled using RANS simulation but it does not predict the fluctuating part of velocity. So to capture the fluctuating part also, either LES or DNS computation is performed according to the need and availability of computational resources. The fluctuating component is generally captured by differencing the instantaneous term and the mean value. Considering three dimensional flow problem with three components of velocity, the CFD software makes the use of tensor with nine components of velocities to understand the relationship of those terms. The tensor also known as Reynolds stresses can be represented as in equation (5).

$$T = \begin{bmatrix} u'u' & u'v' & u'w' \\ u'v' & v'v' & v'w' \\ u'w' & v'w' & w'w' \end{bmatrix} \tag{5}$$

The viscous stress tensor can only dissipate the smaller eddies which are of the size of Kolmogorov's length scale. Hence, extra stress term τ_{sgs} which is known as sub-grid stress is added to increase the dissipation and breaks down the eddies which are just larger than the cell size. τ_{sgs} is calculated using an eddy viscosity model which is given in (6).

$$\tau_{sgs} = 2\rho\nu_{sgs}S^*_{ij} - \frac{2}{3}\rho k_{sgs}\delta_{ij} \tag{6}$$

S^*_{ij} is the strain rate of the resolved eddies on the CFD mesh that depends on the velocity gradient. The stress is able to dissipate the eddies which are just larger than the cell size in the mesh. ν_{sgs} is responsible for the strength of τ_{sgs} that accounts only the size of the eddy and not it's shape. Various sub-grid models are developed that use different methods to solve for ν_{sgs}.

3.1 Smagorinsky model with Van Driest damping

In this project, we are using the Smagorinsky model developed in 1963 which assumes the sub-grid eddies present in the viscous sub-layer. The ν_{sgs} can be calculated using the equation (7)

$$\nu_{sgs} = (C_s\Delta)^2\sqrt{2S_{ij}S_{ij}} \tag{7}$$

C_s is the Smagorinsky coefficient whose default value is 0.68 in OpenFOAM. Δ represents the cubic root of the volume of cell. The dimensional form of the sub-grid viscosity is given in (8)

$$\nu_{sgs} \sim l_0 * u_{sgs} \tag{8}$$

Where l_0 is the integral length scale which is expressed as (9) and u_{sgs} is the corresponding velocity. To model ν_{sgs} near the wall, Van Driest damping function is introduced.

$$l_0 = \min[\kappa y * D, C_s\Delta] \tag{9}$$

D is the Van Driest damping function given by equation (10).

$$D = \left(1 - \exp\left(\frac{y^+}{A^+}\right)\right) \tag{10}$$

where A^+ = 26 and κ = 0.41 which is carefully calibrated for a good agreement with the experimental data.

4 Simulation Procedure

4.1 Geometry and Mesh

The domain is the three-dimensional rectangular channel where the planar jet is entering whose height is half of the channel's height. Lien et al. (2004) recommended for 150 W length for a fully developed turbulent flow in a channel. Considering the simplicity of the geometry, blockMesh is chosen for the construction of the domain and mesh. BlockMesh is an open-source meshing utility available in the OpenFOAM which generates the hexahedral cells. For the creation of geometry for the required case, the available tutorial case of /tutorials/incompressible/pimpleFoam/LES/channel395 is chosen. The geometry consists of 6 blocks considering x-direction as the flow direction, y as the wall-normal or crossflow direction and z as the spanwise direction. The creation of blockMesh can be a bit confusing so the following command made the implementation much easier as it numbers the vertices in paraview.

```
-paraFoam -block -builtin
```

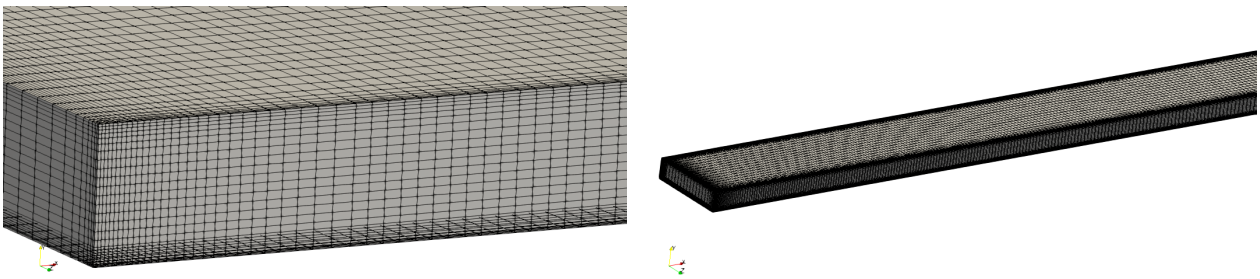

(a) (b)

Figure 3: Section of the mesh

After the creation of the geometry, the most challenging part is the creation of suitable mesh considering the required Kolmogorov's length scale and most importantly available computational power and time for conducting LES simulation. The length of the channel is to be chosen in such a way so that the flow becomes fully turbulent and developed until the flow reaches the given length.

$$C_f = 0.079\ Re^{-\frac{1}{4}} \tag{11}$$

Coefficient of friction (C_f) depends upon the Reynolds number of the flow in an incompressible fluids. Equation (11) is generally used in an internal type of flow which is given by Blausius equation. The wall shear stress is calculated using equation (12) that is useful to evaluate the friction velocity (u_τ). The friction Reynolds number (Re_τ) which is thus, calculated using (14) is required to compare the LES results with DNS calculations performed by Pope (2011).

$$\tau_w = \frac{1}{2}\rho U^2\ C_f \tag{12}$$

$$u_\tau = \sqrt{\frac{\tau_w}{\rho}} \tag{13}$$

$$Re_T = \frac{u_\tau W}{\nu} \tag{14}$$

$$\Delta x = \frac{\Delta x^+\ \nu}{u_\tau} \tag{15}$$

Hence,these parameters helps to calculate the cell spacing in the mesh that is given in equations (15). The smallest grid in the domain should be in the order of Kolmogorov's length scale (η) which is generally employed for a DNS calculation. This scale resembles the smallest eddies present in the flow which is a function of Re as given in equation (16). For LES simulation a general trend for the smallest grid height in the geometry is using (2-10)η. This scaling is usually assumed to resolve the turbulent eddies in the flow. The grids used in the present study is explained in table 3. The first cell height of the grid (Δ) at the wall of channel is chosen so that the resolution of 4η criteria is fulfilled for every Re cases which is equivalent to Δ^+=2.2 in each direction. Along with the spatial discretization, table 2 ans 3 also has the details of time discretization or time step of the calculation at every iteration. The mesh for Reynolds number 1200, 1500, 1800 and 2400 is

Table 2: Details of Mesh Configuration for periodic geometry: Δx^+=2.2, Δy^+=2.2 and Δz^+=18

Re	$N_x \times N_y \times N_z$	Δx (first cell height)	Δy (first cell height)	Δz (cell height)	Δt
1200	566×20×22	1.96e-04	1.96e-04	1.8e-03	6.5e-05

Table 3: Details of Mesh Configuration for confined geometry: Δ^+=2.2

Re	$N_x \times N_y \times N_z$	Δ (first cell height)	Δt
1200	566×20×26	1.96e-04	6.5e-05
1500	588×22×28	1.65e-04	5.0e-05
1800	630×26×30	1.44e-04	3.6e-05
2400	670×28×40	1.16e-04	2.8e-05

created in order to study fully developed nature of the flow. Thus, Re_τ is calculated using equation (14) as 98, 120, 140 and 180 respectively. The mesh details is given in table (2, 3).

$$\frac{\eta}{W} = Re^{-\frac{3}{4}} \tag{16}$$

The geometry is created using 6 blocks and refinement is added at the interface between jet and rectangular channel. In order to capture the inlet of the jet sharply, additional refinement is added at the inlet along mean flow direction at first 20 mm and then uniformly distributed up to 1.5 m. A fine refinement is added near the walls of the confined geometry using simpleGrading input parameter in the *blockMeshDict* file. The periodic case for $Re = 1200$ contains its periodicity in the spanwise direction. So, the mesh is uniformly distributed for this case in that direction. Meanwhile, for all other confined cases, due to the presence of wall bounded geometry, the mesh should be constructed considering the inflation layers near the walls of the channel.

4.2 Initial and Boundary Conditions

In order to simulate the planar jet opening in a rectangular channel with aspect ratio (A) of 0.25 defined in equation (17), periodic case is introduced initially for $Re = 1200$ case in the spanwise direction and the methodology to be adopted is studied for LES. Gohil et al. (2012) discusses the significance of imparting perturbation even at a low-Reynolds number jet inlet case. Author also adds that the laminar regime in the jet flow contains some of the fluctuations showing turbulence characteristics. Payri et al. (2016) makes a detailed study of inlet condition of jet to produce more coherent turbulent structures and adequate velocities. According to the paper, the fluctuating boundary condition available in OpenFOAM over estimates the velocity decay although giving acceptable results. Therefore, turbulentInlet boundary condition is used to produce the fully developed turbulent flow in the channel.

$$A = \frac{W}{S} \tag{17}$$

4.2.1 Inflow boundary condition

For a LES simulation, it is necessary to perturb the flow at the inlet itself to get the fully developed and turbulent flow in the required regime. It is conventionally performed using fluctuations superimposed to the mean velocities. Realistic inflow condition is necessary because it may affect the downstream turbulent characteristics according to Klein et al. (2003). The project makes the use of turbulentInlet boundary condition available at OpenFOAM which produces the spatiotemporal-variant field by summing a set of pseudo-random numbers. Pseudo random number means that they are deterministic but would pass a random number test. They produce the same set of random number after a long interval as the seed or initial value is hard coded in the OpenFOAM. The velocity components in all 3 directions are added with the same random number as (u+R,v+R,w+R), where R represents the randomized number. The patch field (x_p) in the CFD code is calculated using equation (18). The pseudo random number is generated using a Gaussian probability distribution and added to the three components of velocities. The inlet profile of the channel is plotted with the velocity vector (see figure 4).

$$x_p = (1 - alpha){x_p}^{n-1} + \overbrace{alpha}^{scalar=0.1} *(x_{ref} + c * s * R * |x_{ref}|) \tag{18}$$

where:

c is correction term.

s is RMS fluctuation scale.

R is a pseudo-random number.

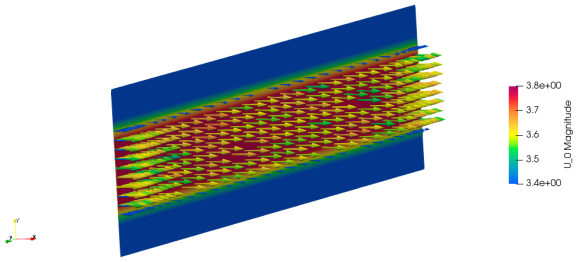

Figure 4: Inlet Velocity Vector for $Re = 1200$

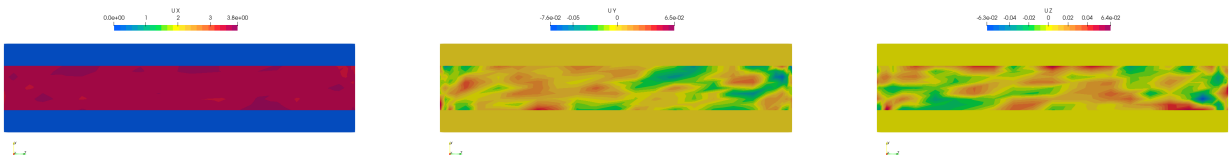

(a) $x - component(u)$ (b) $y - component(v)$ (c) $z - component(w)$

Figure 5: Contours of inlet velocity of $Re = 1200$

4.2.2 Numerical boundary condition

Boundary condition is an important condition that decides the type of the simulation that is being performed. Using Smagorinsky model to simulate the problem, only three parameters is needed to be described which are velocity (U), kinematic pressure (p) and turbulent kinematic viscosity (nut).

Table 4: Boundary condition for U

Patch	Condition	Value (ms^{-1})
Inlet	turbulentInlet	RMS=0.04
Outlet	inletOutlet	(0, 0, 0)
Top & Bottom	fixedValue	(0, 0, 0)
Front & Back	fixedValue	(0, 0, 0)

Table 5: Boundary condition for p

Patch	Condition	Value (m^2s^{-2})
Inlet	zeroGradient	-
Outlet	fixedValue	0.0
Top &Bottom	zeroGradient	-
Front & Back	zeroGradient	-

Table 6: Boundary condition for nut

Patch	Condition	Value (m^2s^{-1})
Inlet	zeroGradient	-
Outlet	zeroGradient	-
Top &Bottom	zeroGradient	-
Front & Back	zeroGradient	-

4.3 Solver

4.3.1 Numerical Solvers

The NS equation given in equation (2,3) is highly non-linear and hence, it becomes difficult to solve it analytically. So, computational techniques are preferred to solve such kind of problems. Various methods have been developed with the advancement in the computing technologies to solve such types of problem. Finite Difference, Finite Element and Finite Volume methods are the most commonly known and used techniques to solve such a high dimensional and complex problems. These methods requires the discretization of the domain into small basic geometrical elements such as triangles, quadrilaterals in two dimension and tetrahedral, hexahedral in three dimensions which often known as mesh or grids as explained before. In OpenFOAM, Finite Volume approach is used to solve a certain numerical problems. After creation of mesh structures, the next important step is solving the Navier Stoke's equations on those individual cells. The type of numerical solvers and schemes used during solving those problems is vital in the accuracy and stability of the solution. Hence, the solvers used for this project is given in table (7).

Table 7: Numerical Solvers

Field	Linear Solver	Smoother	Tolerance
U	Smooth Solvers	Gauss Seidel Smoother	1e-06
p	GAMG Solver	Gauss Seidel Smoother	1e-05
nut	Smooth Solvers	Gauss Seidel Smoother	1e-06

For time marching, backward differencing method is used which is a second order accurate time scheme.

4.3.2 PIMPLE Algorithm

Since, the problem is incompressible which needs to solve the continuity and momentum equations of 1 and 2, it is vital to chose an algorithm that solves these 4 equations and find a solution of 4 unknowns. The unknown quantities are U_x, U_y, U_z and p. p is the kinematic pressure that is the ratio of static pressure and density of the fluid. The momentum equation is highly non-linear and because there is no any specific equation to obtain pressure in an incompressible flow, we propose an iterative algorithm approach to solve the pressure-velocity coupling problem.

$$MU = -\nabla p \tag{19}$$

Equation (19), gives the linear algebraic form of the momentum equation which is also known as momentum predictor. M is the square matrix with known quantities that is obtained using the Finite-Volume approach in OpenFOAM.

$$AU - H = -\nabla p \tag{20}$$

The matrix M is decomposed into diagonal (A) and off-diagonal (H) matrix as in equation (20) Now, the velocity equations are solved using the initial conditions and then needs to satisfy the continuity equation.

$$\nabla.\left(A^{-1}\nabla p\right) = \nabla.(A^{-1}H) \tag{21}$$

Thus, the continuity equation gives an equation for pressure term which when solved gives the pressure field that can be used to correct the velocity field, so that it satisfies the continuity equation. The corrector loop is repeated until the desired residual is achieved for a single iteration. This process is repeated for different time steps as we are solving transient simulation.

The solver we are using to solve this problem is known as PIMPLE algorithm provided by OpenFOAM which is a combination of SIMPLE and PISO algorithms. When the corrector loop is executed only once, the algorithm resembles as the transient SIMPLE whereas if the iteration is conducted only once then the simulation resembles the PISO algorithm. PIMPLE algorithm is chosen so as to increase the consecutive time steps that is compensated by using multiple iterations in the pressure-velocity coupling.

Step 1: The momentum equations are solved from the assumed pressure p which yields the velocity field.

Step 2: The pressure equation is solved using obtained velocity field.

Step 3: Velocity fields are corrected that is obtained from Step 2. 2 and 3 steps act as corrector loop also called innerCorrectors in OpenFOAM.

Step 4: The turbulence related fields are then corrected. Those fields are again used to solve momentum equation on step 1 and looped until desired residual tolerance criteria are met. This is known as pressure-velocity coupling or outerCorrectors.

Step 5: Forward time marching until end time.

```
PIMPLE
{
    nNonOrthogonalCorrectors 0;
    nCorrectors              1;
    nOuterCorrectors        50;

    residualControl
    {
        U
        {
                tolerance  1e-5;
                relTol       0;
        }
        p
        {
                tolerance  5e-4;
                relTol       0;
        }
     }
}

relaxationFactors
{

    equations
    {
        ".*"        1;

    }
}
```

The nOuterCorrectors used in the Pimple Algorithm makes use of large number of corrector loops. This parameter is crucial in differentiating it from the PISO loop. In order to get the converged solution in each Pimple loop, residual control is introduced. Also, the relaxation factor is introduced which is recommended as 1 for transient calculations given in OpenFoamWiki (2006)

5 Results and Discussions

For a LES calculation, we need to consider the mesh size which is able to resolve the larger eddies and model the tiny eddies present in the flow. The time step should be considered in a way so that it captures the required turbulent phenomenon in the domain. So, the Courant-Fell Lewi number is the important parameter to be considered for such simulation which is given in equation (22).

$$CFL = \frac{u_m \Delta t}{\Delta x} \tag{22}$$

Lower the CFL number, higher we can achieve turbulent structures in the flow. Considering the present computational power and usage of PIMPLE algorithm, maximum Courant number is chosen as 1 for the project.

5.1 Velocity Signals and Power Spectrum

In order to simulate a transient flow simulation, the important parameter to observe as an intermediate post-processing step is the probe data according to xu et al. (2003). The velocity signal should be carefully observed at different locations of the domain using probe function object at $controlDict$ file. The data for the signal is started right at the beginning of the simulation i.e. from t=0 second at every time step for each simulation. Hence, the frequency of collection of these data for all cases is at about 15kHz. After the velocity signal attains steady nature of data with similar range of fluctuations, collection of mean and statistics needs to start so that the mature results are obtained faster. In the velocity signal plot, it can be seen that steady nature of data with similar range of fluctuation starts after t=0.6 second. The velocity signal for $Re = 1200$ at (0.1, 0, 0)m in the channel is plotted in figure (6).

To understand the turbulent flow from the jet, power or energy spectrum of the velocity signal near jet inlet is studied. The spectrum is obtained using the data of the velocity signals and fast fourier transforming (FFT) those data and is plotted in log-log scale. The significance of the energy spectrum is that this provides information about the magnitude of the eddies as it evolves or dissipates through time. The larger eddies in the flow at particular instant of time is attributed by large scale and the dissipation scale is when the eddies are damped out. The inertial sub-range as shown in figure (6d) signifies the magnitude of the flow to be of turbulent nature or not at a particular location. This power spectrum is plotted using the velocity signal shown in figure (6) and fast fourier transforming those data using the python code given in appendix J.

In figure (7a), the velocity plot is seen to be almost constant for $Re = 1200$ case. It suggests that the flow is already damped out at this position i.e. (0.5, 0, 0)m and there is almost no fluctuation in its mean velocity component. The other component of velocity is fluctuating although the value is very less. On comparison between $Re = 1200$ case at two different location of the channel in figure (6 and 7), it is observed that the fluctuation in y and z component of velocity is much larger when the flow is closer to the jet. Hence, for $Re = 1200$ the turbulence generated by the planar jet is already damped out in the flow at this location. Further, signals at same location is plotted for different Reynolds number shown in figures (8, 9 and 10). The fluctuation in the mean flow direction increases with the increasing Reynolds number. The power spectrum is plotted for each

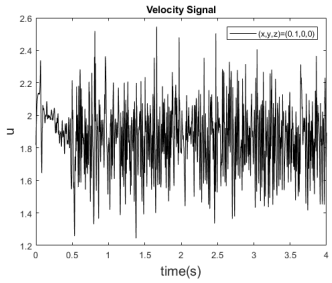

(a) $x - component(u)$

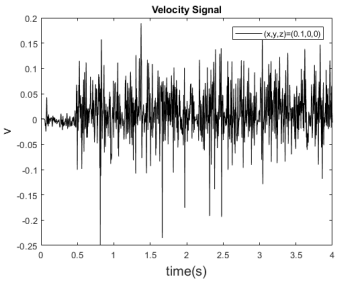

(b) $y - component(v)$

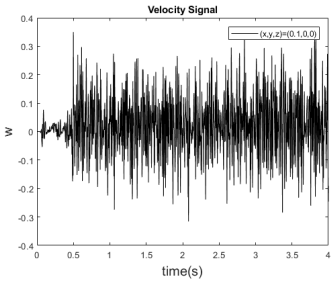

(c) $z - component(w)$

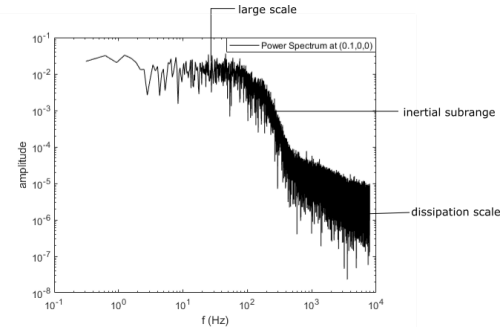

(d) Power Spectrum

Figure 6: Velocity Signal at (0.1,0,0)m of $Re = 1200$

signals and it can be seen that the slope of the spectrum tend to decrease at the inertial subrange region as the flow moves further downstream when eddies gets dissipated.

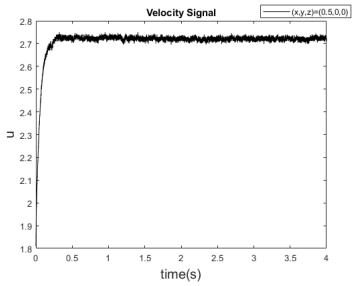

(a) $x - component(u)$

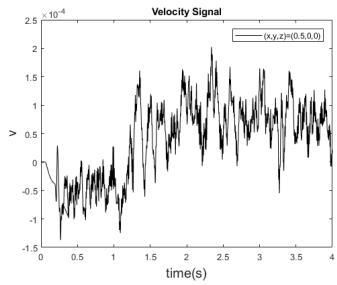

(b) $y - component(v)$

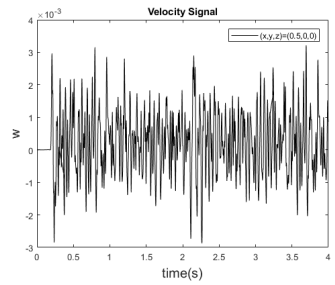

(c) $z - component(w)$

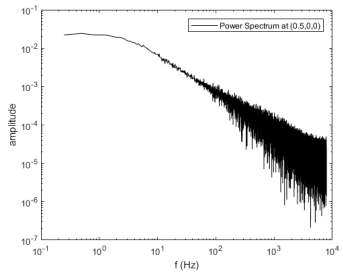

(d) Power Spectrum

Figure 7: Velocity Signal at (0.5, 0, 0)m of $Re = 1200$ and Power Spectrum

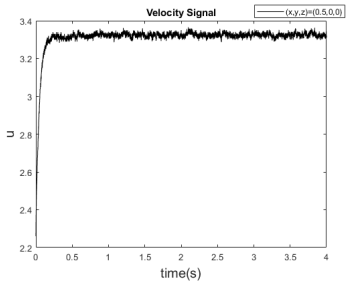

(a) $x - component(u)$

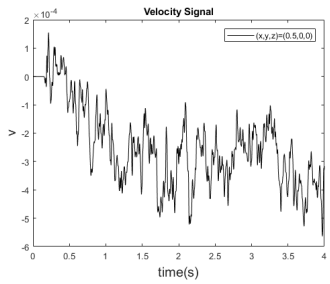

(b) $y - component(v)$

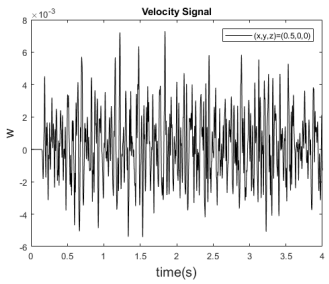

(c) $z - component(w)$

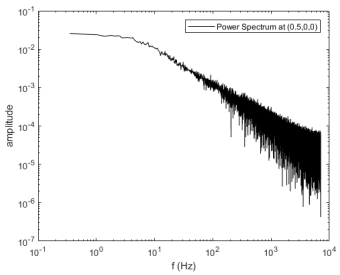

(d) Power Spectrum

Figure 8: Velocity Signal at (0.5, 0, 0)m of $Re = 1500$ and Power Spectrum

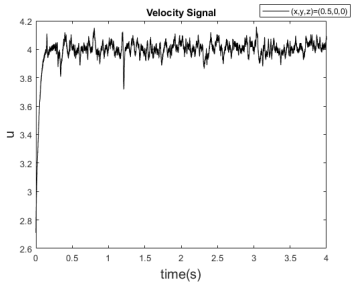

(a) $x - component(u)$

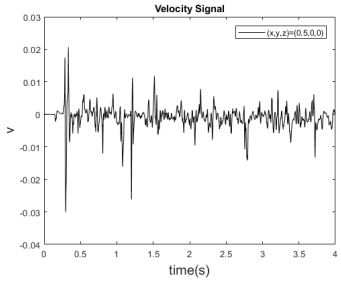

(b) $y - component(v)$

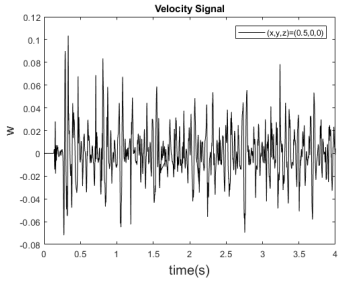

(c) $z - component(w)$

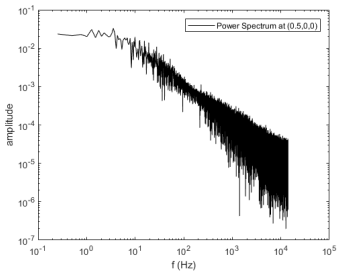

(d) Power Spectrum

Figure 9: Velocity Signal at (0.5, 0, 0)m of $Re = 1800$ and Power Spectrum

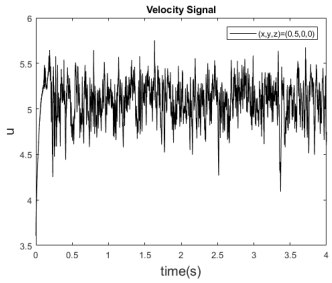

(a) $x - component(u)$

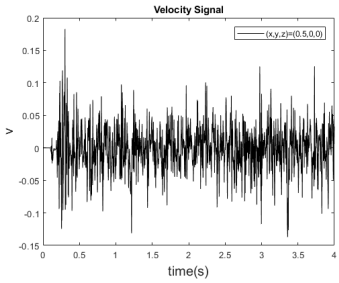

(b) $y - component(v)$

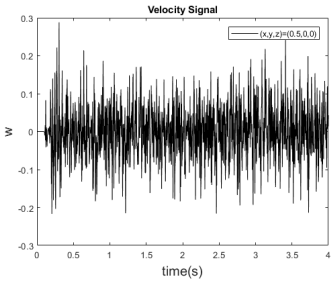

(c) $z - component(w)$

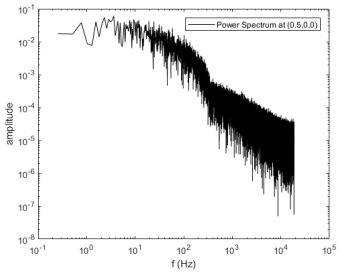

(d) Power Spectrum

Figure 10: Velocity Signal at (0.5, 0, 0)m of $Re = 2400$ and Power Spectrum

5.2 Secondary Flow

With the primary flow in the longitudnal or x-direction of the channel there may be existence of secondary flow in corresponding cross flow and spanwise axes. This type of characteristic flow is predominantly seen in the turbulent regime. In the laminar flow, the flow is primarily along the longitudnal axis. So, the contour plots in the cross-section of the channel would aid to determine the type of flow. The figure in (11) shows secondary flow for $Re = 1200$ at different location near the planar jet in the channel and at downstream. The magnitude of these flows is shown in the index bar of each figure whose values decreases as those section moves downstream of the flow. At x=0.01 which is right after the jet flow, the magnitude are maximum which suggest the flow to be chaotic or turbulent and decreasing magnitude helps to decide that the turbulence is damped out.

Also, similar plots are constructed for different Reynolds number in appendix B where similar trend in the flow is observed. The important observation is that the turbulence nature persists at much longer length of the channel in the flow if the Reynolds number taken is much larger. Meanwhile, in order to understand and visualize the secondary flow in its full phase, a cross-sectional profile is shown in figure (12) where the contour is given for the mean flow and the velocity vectors is shown without any scale factor. This cross sectional view of secondary flow is given for $Re = 1200$ at x=1.4m after the flow is fully developed.

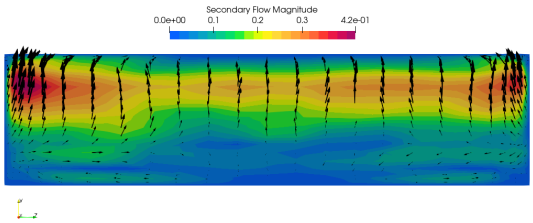

(a) x=0.01m

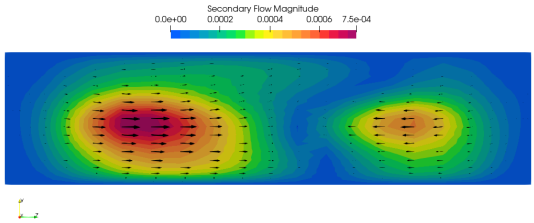

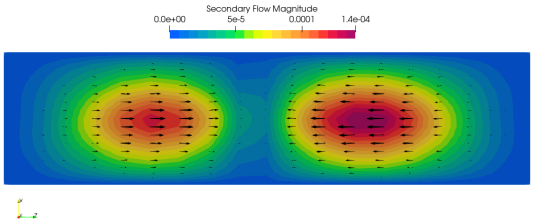

(b) x=0.75m (c) x=1.4m

Figure 11: Secondary flow for $Re = 1500$

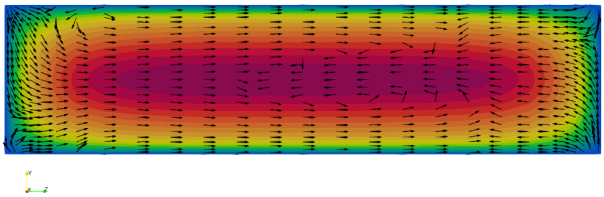

Figure 12: Secondary Flow vector plot without scaling

5.3 Isosurface of Q-criteria

Q-criteria is one of the popular technique used in CFD in order to visualize the coherent vortical structures in the flow. It is the value that can be calculated using the instantaneous velocity fields. Moreover, this criteria is based on the gradient of unstructured data set which is usually taken as velocity in the flow. Hence, the criteria is defined as in equation (23) which is a magnitude of relative difference between vorticity(ω) and strain tensor(S). Also, Q-citeria is known as the second invariant of the rate of deformation tensor. Isosurface is the way of visualizing or representing the surface of any scalar function that does not vary or is constant such as Q-criteria.

$$Q = \frac{1}{2}(trace(\omega)^2 - trace(S)^2) \tag{23}$$

In the figure (13), the turbulent eddies in the flow for all the cases is seen using Q-criteria function in paraview at fully developed condition when t=4s and x=1.4m downstream of the channel. For all Reynolds number, the same value of isosurface is used as 500 while plotting so that the results can be analysed. For $Re = 1200$, the turbulent eddies is damped out as soon as it flows from the jet at around 0.1m downstream. Similarly, in $Re = 1500, 1800$ and 2400 the eddies is dissipated at around 0.15m, 0.3m and 0.6m respectively. Also, the positive value of isosurface of Q-criteria represents the dominance of rotating component of velocity or vorticity over the stretching component. Therefore, the contours shown in the figure demonstrates that the vortices in the flow field dominates the strain rate.

5.3.1 Evolution of jet in the channel and its characteristics

In order to visualize the nature of the jet at the inlet of the channel, isosurface of q-criterion is used since capturing the characteristics of the jet is very critical. The height of the channel being double the jet inlet, a suction pressure (see figure 14) is created between the vacuum and fluid right after the inlet in every cases. At t=0.01s for $Re = 1200$ case, it can be seen that the jet just started to penetrate creating vortical structures from the jet at subsequent time. The vortices are also seen to be generated from the wall surface and entrainment of fluid is visualized when marching ahead in time. Along with case of $Re = 1200$, the evolution of jet in time for different Reynolds number is shown in appendix C.

Also, the streamlines of the jet is captured at the inlet for all Reynolds number cases at t=4s and the length of the recirculation region seems to vary with increasing Reynolds number. For $Re = 1200$ in the figure (15a), the length of the recirculation region is seen to be around 0.025m from the inlet. Subsequently, the maximum length of these regions for $Re = 1500$ is 0.03m, $Re = 1800$ is 0.035m and for $Re = 2400$ is about 0.05m (see figure 15b, 15c and 15d respectively). Multiple number of the recirculation zones is present for $Re = 2400$ case which signifies the suction pressure is increasing with the increase in the velocity of the jet.

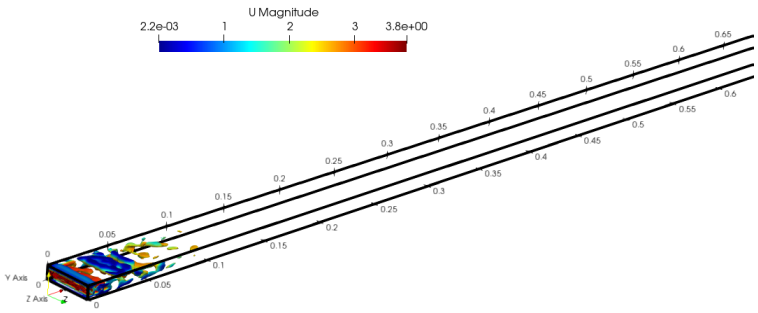

(a) $Re = 1200$

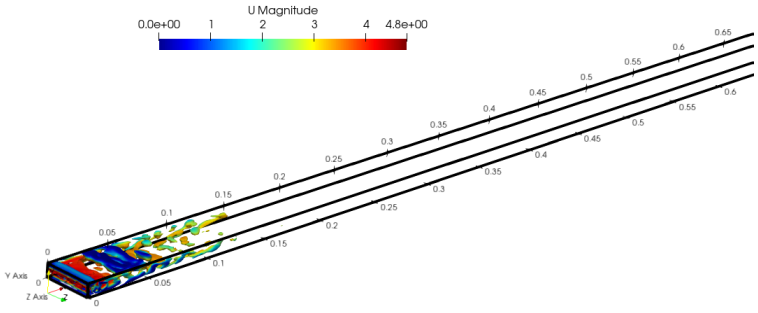

(b) $Re = 1500$

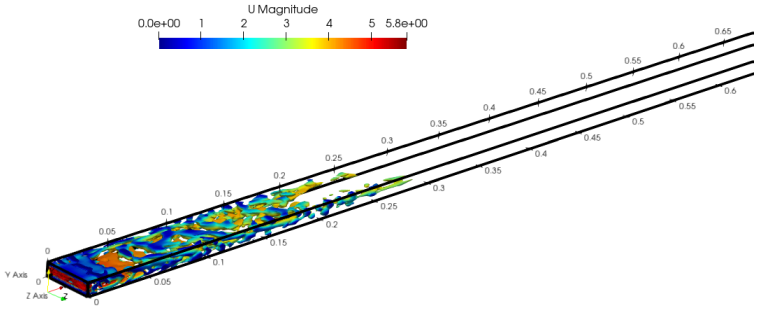

(c) $Re = 1800$

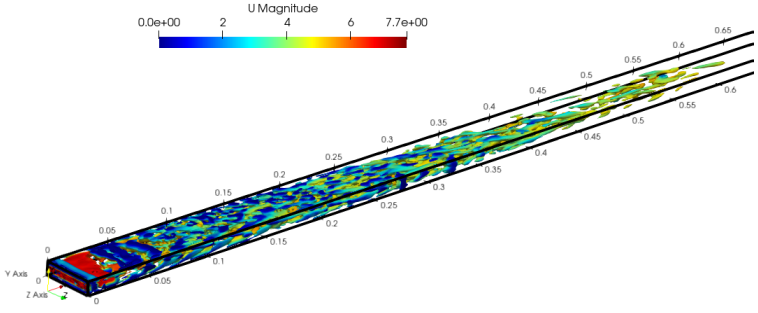

(d) $Re = 2400$

Figure 13: Isosurface of Q-criterion with value 500 at fully developed condition

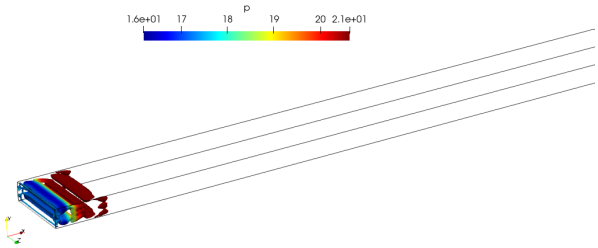

(a) t=0.01s

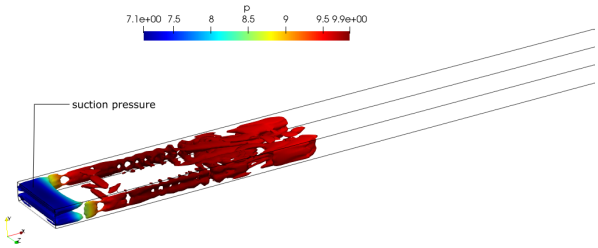

(b) t=0.05s

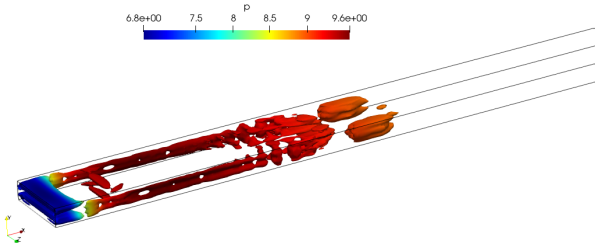

(c) t=0.1s

Figure 14: Isosurface of Q-criteria with value 200 for $Re = 1200$

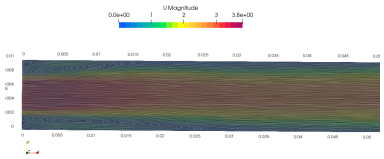

(a) $Re = 1200$

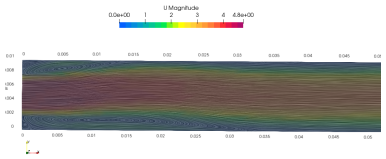

(b) $Re = 1500$

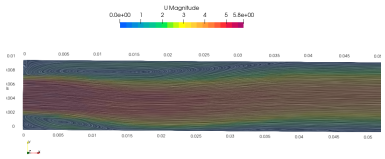

(c) $Re = 1800$

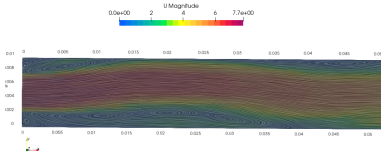

(d) $Re = 2400$

Figure 15: Streamlines of the jet at t=4s

5.4 Mean Velocity

When the field-averaging in the simulation gets started, the mean profiles are the ones that first attains the converged results. The procedure to check if the data is matured is usually with the usage of plot over line utility in Paraview, a post-processing application. A convergence criteria for space and time should be analysed to see a minimum changes in the plot. Also, the outcome for a channel flow the mean and statistical profiles is assumed to be symmetrical.

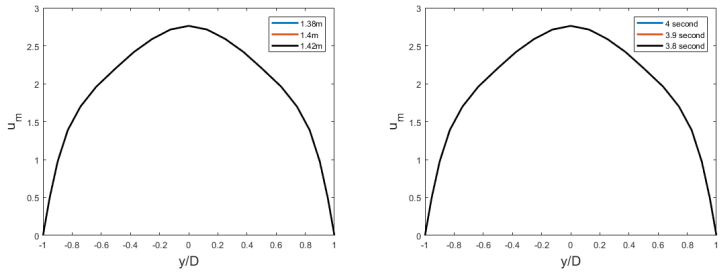

Figure 16: Mean Velocity Profiles of $Re = 1200$ (confined). From left to right: spatial and time convergence

For a spatial convergence criteria, 3 different positions at x=1.38m, 1.4m and 1.42m when t=4s along the mean flow direction is taken where mean velocity magnitude vs y/D is plotted at the midplane of the channel. Meanwhile, to validate the temporal convergence, 3 different time-steps at t=3.8, 3.9 and 4 seconds is plotted at 1.4m downstream of the flow direction. It is observed that for the simulated Reynolds number as shown in the figure (16) for a confined case of $Re = 1200$, the convergence criteria is fulfilled. The plot of the other simulated Reynolds number is shown below in the appendix D. Also, usually for an unsteady simulation it is often seen that the mean quantities are converged at first and only then the statistics gets steady results. The mean velocity profile in the plot seems to be parabolic. This suggests that the flow might be laminar. Convergence in spatial and temporal domain suggested the flow to be fully developed at the given location around x=1.4m and t=4s. Therefore, in order to validate the result from the simulation, experiment conducted at the lab facility of IIT Bombay was employed for the validation of the simulation results at low-Reynolds number cases at $Re = 1200$. The data was collected at the fully developed region at the midplane in the duct. Hence, the plot showing the mean velocity profiles in figure (18) with the standard deviation given in green colour bar helps for the validation of the simulation result.

In the study done by Theofilis et al. (2004), the authors developed analytical technique for a fully developed laminar flow in a confined rectangular channel with variable A. Two dimensional Poiseuille flow is retrieved in the y-direction when the series term in the equation is converged for A tending to 0. To validate the analytical formula in the paper with the simulation, a case with $Re = 100$ is used which is surely a case of laminar flow. The analytical formula is given in equation (24).

$$U\left(Y_o, Z_o\right) = \left(1 - Y_o^2\right) + \sum_{n=0}^{\infty} \frac{32(-1)^n \cosh\left\{\frac{(2n+1)\pi Z_o}{2}\right\}}{(2n+1)^3 \pi^3 \cosh\left\{\frac{(2n+1)\pi}{2A}\right\}} \times \cos\left\{\frac{(2n+1)\pi Y_o}{2}\right\} \tag{24}$$

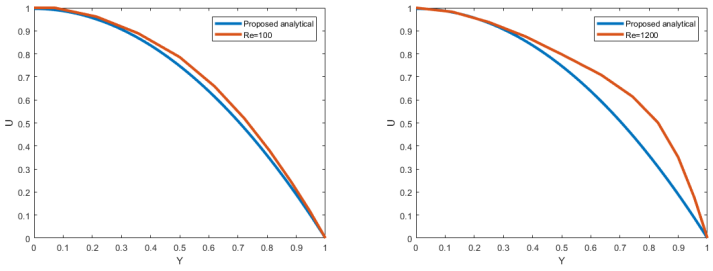

Figure 17: comparison of proposed analytical velocity profiles.From left to right: $Re = 100$ and 1200

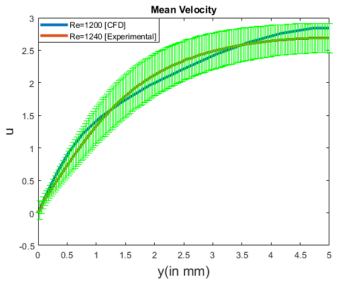

Figure 18: comparison of experimental velocity profiles with simulated case of $Re = 1200$

U, Y_o and Z_o in the formula is normalized as shown in equation (25) and the plot showing velocity profiles for proposed analytical, $Re = 100$ almost perfectly fits the analytical plot although the case with $Re = 1200$ does not perfectly agree with the plot as given in figure (17). The reason might be due to some assumption made during the derivation of the formula or due to the boundary layer effect near the walls being the confined channel case. Anyway, from the plots showing the velocity fluctuation given below is almost negligible at the developed region. Hence, for this case the eddies might get dissipated at downstream of the channel which can also be concluded from the isosurface plots.

$$U = \frac{u}{u_{max}}, \qquad Y_o = \frac{2y}{W}, \qquad Z_o = \frac{2z}{S} \tag{25}$$

Since, the rectangular channel is confined which is bounded by the walls, the mean velocity profiles should be analysed along cross-flow as well as spanwise direction. The graphs plotted at variable Y and Z respectively help to understand the boundary layer effect by the walls in the flow. The mean velocity profile along the shortest dimension i.e. height(y) of the channel is sort of parabolic in nature whereas along the longer dimension in cross-section, the profile is flat. On a detailed observation of the plots, it can be seen that the profile tend to grow steeply near the walls along Y with increasing Reynolds number cases which indicate that the eddies near the wall persists in the flow for higher Re case that is being simulated. The family of curve is plotted along Y and Z respectively varying the location in the channel at fully developed mean flow position i.e. x=1.4m. The velocity profile is decreased as the location is shifted near the walls for both cases along Y and Z which indicate the effect of walls on the flow regime.

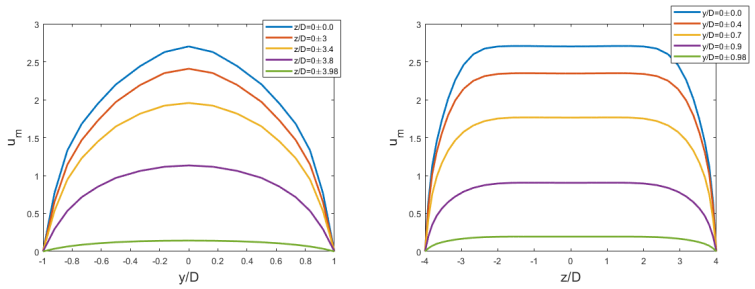

Figure 19: Mean Velocity Profiles of $Re = 1200$ (confined). From left to right: along Y at different Z and along Z at different Y

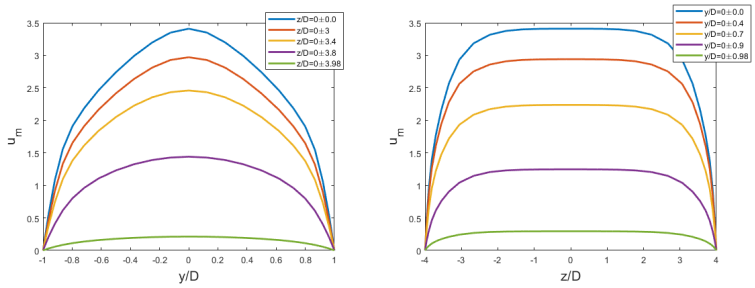

Figure 20: Mean Velocity Profiles of $Re = 1500$ (confined). From left to right: along Y at different Z and along Z at different Y

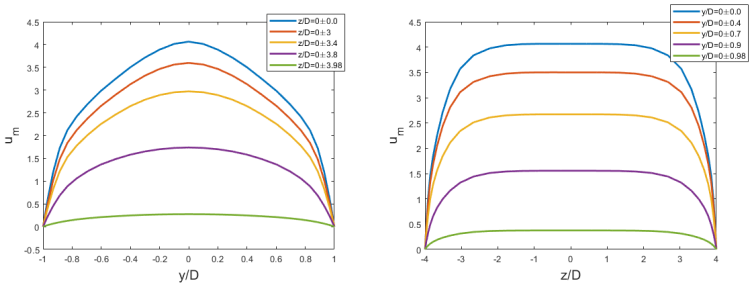

Figure 21: Mean Velocity Profiles of $Re = 1800$ (confined). From left to right: along Y at different Z and along Z at different Y

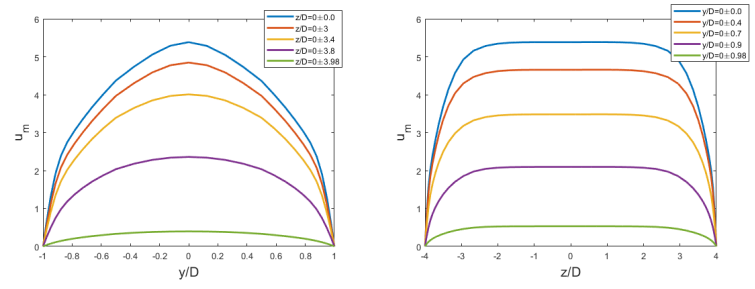

Figure 22: Mean Velocity Profiles of $Re = 2400$ (confined). From left to right: along Y at different Z and along Z at different Y

5.5 Velocity Fluctuations

As discussed earlier, in equation (4) the instantaneous velocity is a combination of mean and fluctuating parts. Hence, it is essential to analyze the fluctuating components via the plots. The Reynolds stress terms in the principal diagonal of stress tensor are $< u'u' >$, $< v'v' >$ and $< w'w' >$. The root mean square (rms) of these components are normalized fluctuating parts of velocity. In order to normalize, the ratio of u^{rms} to the channel averaged velocity (u_m) is taken for respective Reynolds number. The plots in figure (23 and 24) shows the spatial and time convergence plots at the midplane of the channel in the fully developed region for $Re = 1200$. The convergence plots for higher Reynolds number are given in appendix E.

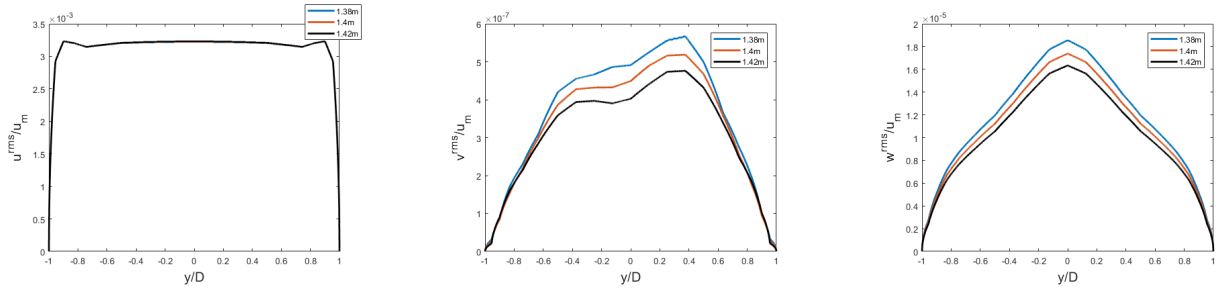

(a) $\frac{u^{rms}}{u_m}$ (b) $\frac{v^{rms}}{u_m}$ (c) $\frac{w^{rms}}{u_m}$

Figure 23: Profiles of fluctuating velocity of $Re = 1200$ for spatial convergence

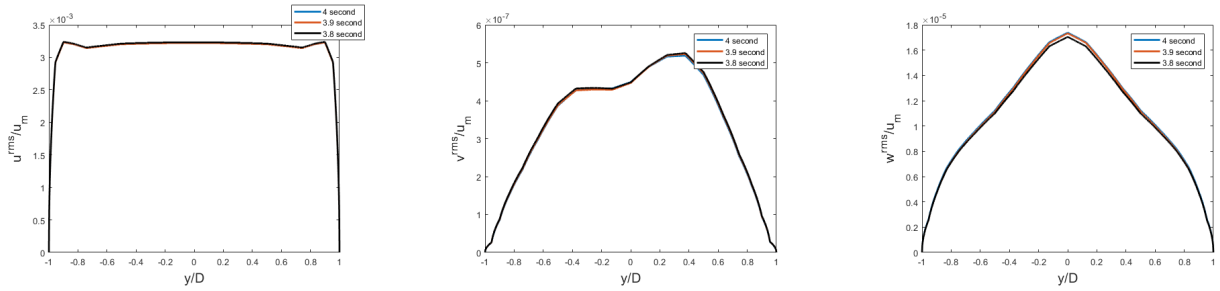

(a) $\frac{u^{rms}}{u_m}$ (b) $\frac{v^{rms}}{u_m}$ (c) $\frac{w^{rms}}{u_m}$

Figure 24: Profiles of fluctuating velocity of $Re = 1200$ for temporal convergence

5.6 Turbulent shear stress

The off-diagonal elements of the Reynolds stress tensor are the turbulent shear stresses given as $< u'v' >$, $< u'w' >$ and $< v'w' >$. The plots are given for a normalized shear stresses against the wall normal direction or height of the channel. This is done using the ratio of respective shear stress with the square of channel averaged velocity (u_m) for respective Reynolds number. The plots in figure (25 and 26) shows the spatial and time convergence plots at the midplane of the channel in the fully developed region for $Re = 1200$. The convergence plots for higher Reynolds number are given in appendix F.

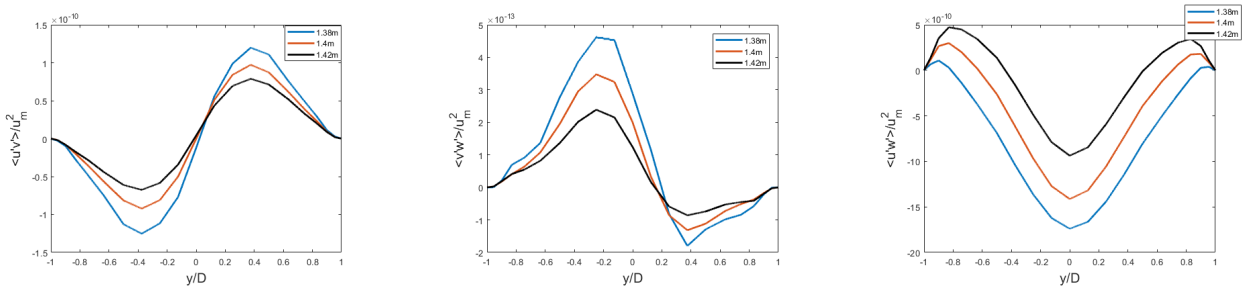

(a) $\frac{<u'v'>}{u_m^2}$ (b) $\frac{<v'w'>}{u_m^2}$ (c) $\frac{<u'w'>}{u_m^2}$

Figure 25: Turbulent shear stress components of $Re = 1200$ for spatial convergence

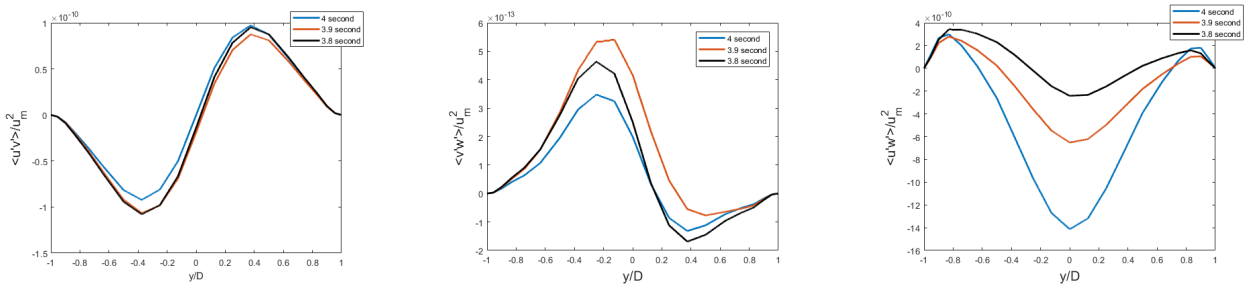

(a) $\frac{<u'v'>}{u_m^2}$ (b) $\frac{<v'w'>}{u_m^2}$ (c) $\frac{<u'w'>}{u_m^2}$

Figure 26: Turbulent shear stress components of $Re = 1200$ for temporal convergence

5.7 Turbulent Kinetic Energy

An important parameter to analyze during a LES calculation is the turbulent kinetic energy (TKE) in the flow field. Larger eddies has larger energy and the kinetic energy is almost zero for small eddies. Hence, assuming no eddies or very tiny eddies in the laminar flow, the TKE is almost zero or infinitesimal. The energy of the eddies in the flow is also described previously from the power spectrum plot.

The contours of TKE at different location of yz cross-section for $Re = 1200$ is shown in figure (27). It is seen that when x=0.1m which is near the inlet of the channel, the magnitude of this quantity is maximum because of existence of eddies from the jet. This also aids to decide the flow

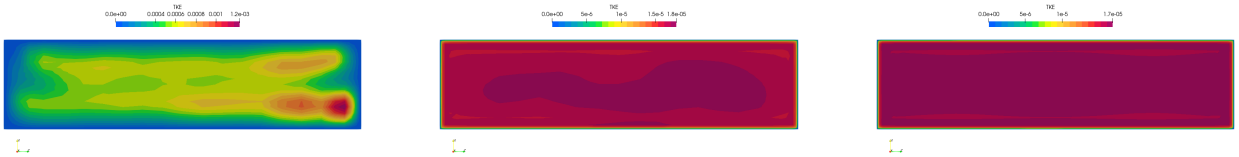

(a) x=0.1m (b) x=0.75m (c) x=1.4m

Figure 27: Turbulent Kinetic Energy profiles for $Re = 1200$

is turbulent in this region. Further, moving downstream of the channel the value keeps decreasing to zero that concludes the flow may be damping out. Along with it, the contours for $Re = 1500$,1800 and 2400 are also given in appendix H. As the Reynolds number increases the magnitude of TKE is further increased that suggests for the production of larger eddies for those simulations.

6 comparison between confined and periodic domains

The comparison for the periodic and confined case at the fully developed region at x=1.4m downstream is made for $Re = 1200$. It is seen that the mean velocity magnitude for a confined case is greater than that of periodic case along the cross flow direction. Also, the fluctuating part of velocity in the mean flow direction is dominant in the confined case. But, the remaining fluctuating components on each direction is less than periodic case as seen in the plots (see figure 28c and 28d). And, in the plot showing turbulent shear stress, the case with confined geometry has larger value in comparison with periodic case which is evident due to presence of wall in the spanwise direction.

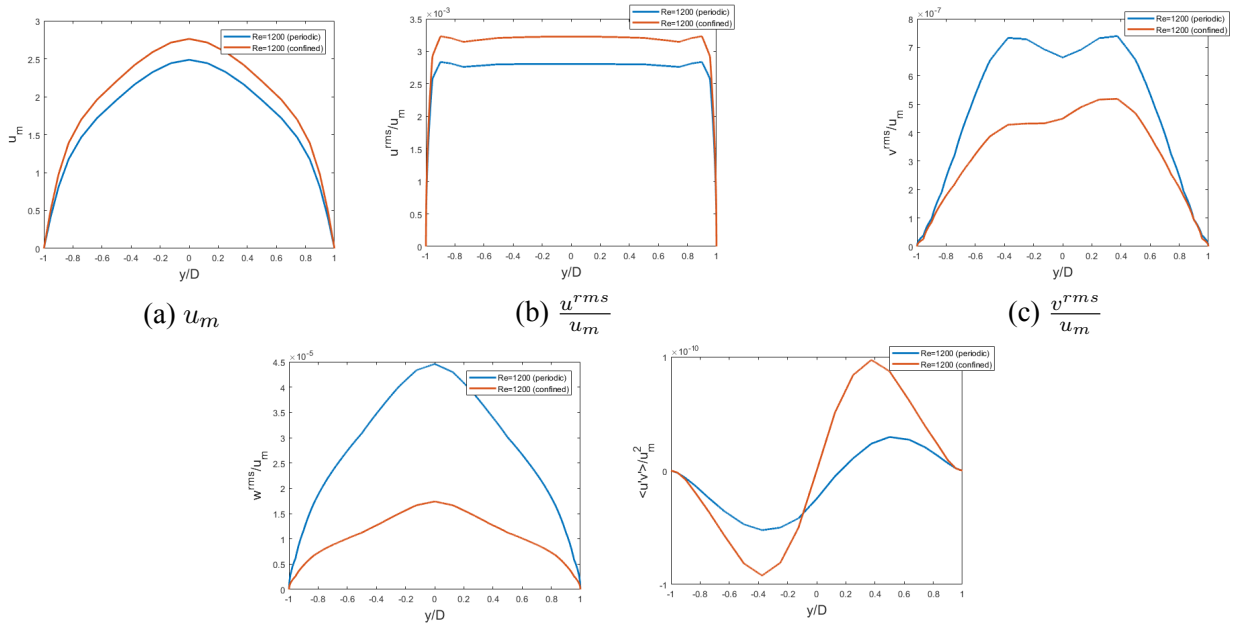

(a) u_m (b) $\frac{u^{rms}}{u_m}$ (c) $\frac{v^{rms}}{u_m}$

(d) $\frac{w^{rms}}{u_m}$ (e) $\frac{<u'v'>}{u_m^2}$

Figure 28: comparison between confined and periodic for $Re = 1200$

6.1 Conclusion

The simulation is conducted for a range of Reynolds number of 100-2400. Due to the application of jet at the inlet of the channel, even at low Reynolds number turbulence characteristics in that region needs to be considered. However, the flow might persists its turbulence nature or may damp out and behave as laminar flow at downstream of the jet in the channel. A detailed study of the planar jet in the channel is made for the transition regime including Reynolds number 1200, 1500, 1800 and 2400. After the intermediate analysis of the simulation, it was seen that the temporal convergence was achieved within 4 seconds. The flow seems to be fully developed near the outlet of the channel at around 1.4 meters or above for all Re. The contours of isosurface is another way to visualize the vortices in the flow or its turbulent characteristics. Therefore, the plot for different Re in figure (13). is evident that the turbulent eddies from the jet dies out further downstream of the flow. As seen in the figure, the fluctuations at this location is very less which suggest that the turbulence from the jet maybe damped out downstream of the channel.

Therefore, from the plots in figure (16, 23, 24, 25, 26) and in appendix D, E and F, it can be seen that for all Reynolds number the temporal convergence is achieved until 4 seconds of simulation whereas for the spatial convergence, the plots doesn't seem to be strictly overlapping. The reason for this maybe due to the small values of the Reynolds stress components or laminar flow in the fully developed region. Also, the other observation from the velocity signal of the probe in figure (6) is that the steady nature of data with similar range of fluctuations starts almost after 0.6 second, hence, collection of mean and statistics is started at this point in time to attain mature data. The streamlines plot at t=4s in figure (54) near the inlet of the channel shows that the recirculation region resulting from the jet varies with corresponding Reynolds number. Higher the Reynolds number, greater is the length of the region of recirculation.

Acknowledgement

I would like to express my sincere gratitude and respect towards Prof. Manaswita Bose, IIT Bombay for constantly supporting and guiding me till the completion of project in the internship. Also, I am very grateful to Mr. Ashley Melvin and Mr. Divyesh Variya for helping me out with every doubts and problems which I had to tackle on this period.

I am extremely thankful towards the supercomputing facility at Kathmandu University and FOSSEE at IIT Bombay, for providing access to its High Performance Computing facilities without which I wouldn't be able to complete the project.

Appendix A Velocity contour plots at xz-plane

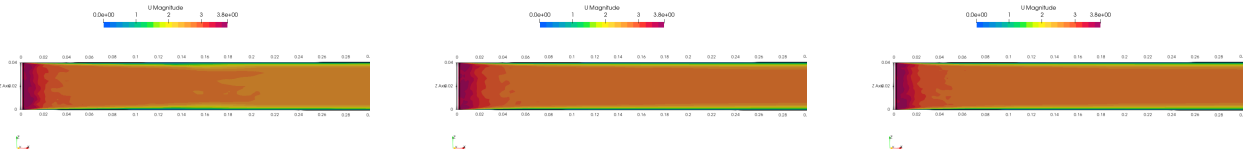

(a) t=0.1s (b) t=2s (c) t=4s

Figure 29: Velocity contour plots of $Re = 1200$

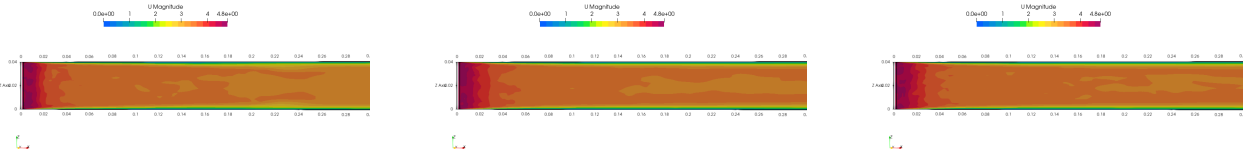

(a) t=0.1s (b) t=2s (c) t=4s

Figure 30: Velocity contour plots of $Re = 1500$

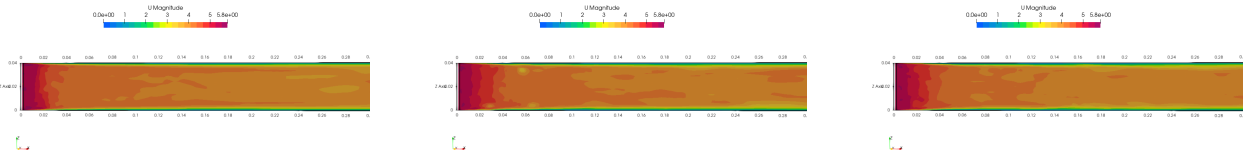

(a) t=0.1s (b) t=2s (c) t=4s

Figure 31: Velocity contour plots of $Re = 1800$

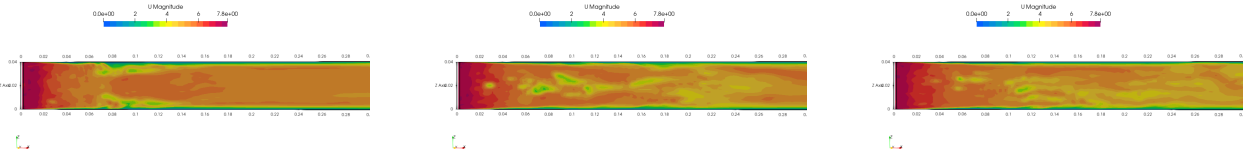

(a) t=0.1s (b) t=2s (c) t=4s

Figure 32: Velocity contour plots of $Re = 2400$

Appendix B Secondary flow at different cross-section of channel

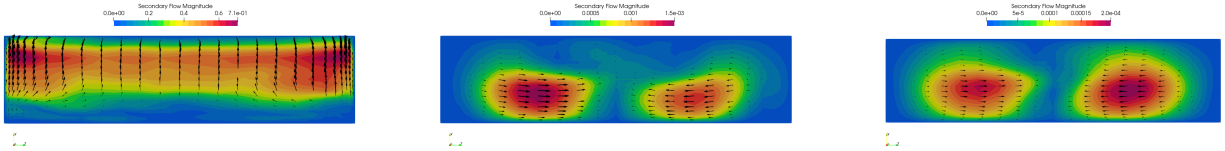

(a) x=0.01m (b) x=0.75m (c) x=1.4m

Figure 33: Secondary flow for $Re = 1500$

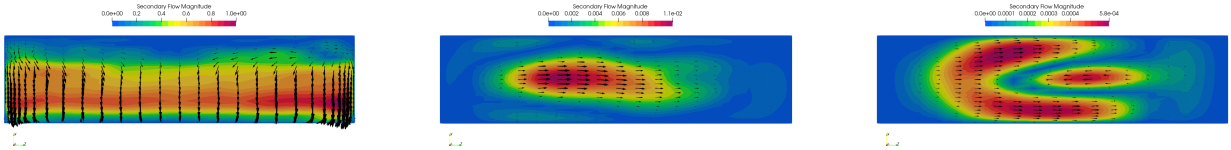

(a) x=0.01m (b) x=0.75m (c) x=1.4m

Figure 34: Secondary flow for $Re = 1800$

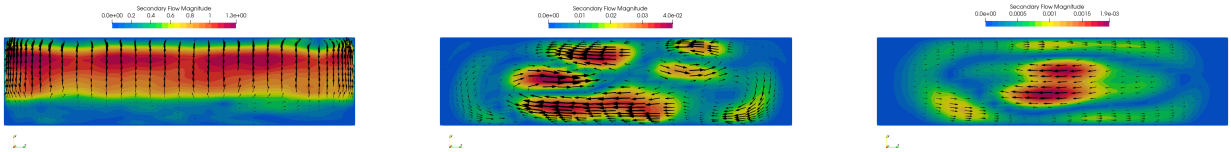

(a) x=0.01m (b) x=0.75m (c) x=1.4m

Figure 35: Secondary flow for $Re = 2400$

Appendix C Evolution of jet

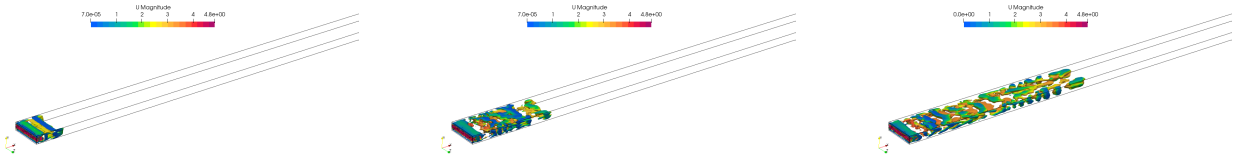

(a) t=0.01s (b) t=0.05s (c) t=0.1s

Figure 36: Isosurface of Q-criteria with value 200 for $Re = 1500$

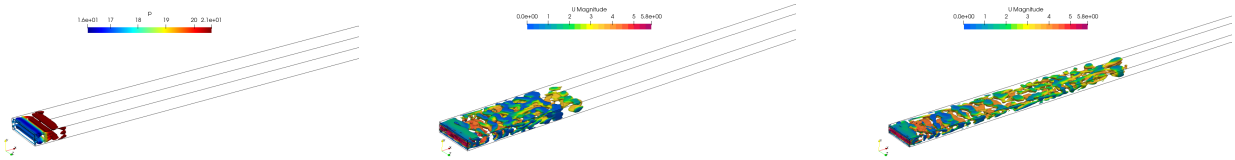

(a) t=0.01s (b) t=0.05s (c) t=0.1s

Figure 37: Isosurface of Q-criteria with value 200 for $Re = 1800$

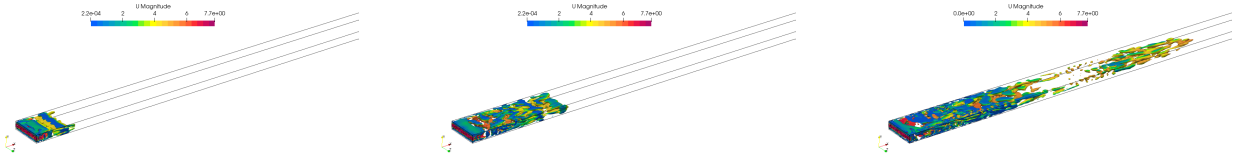

(a) t=0.01s (b) t=0.05s (c) t=0.1s

Figure 38: Isosurface of Q-criteria with value 200 for $Re = 2400$

Appendix D Mean Velocity Profiles for $Re = 1500, 1800$ and 2400

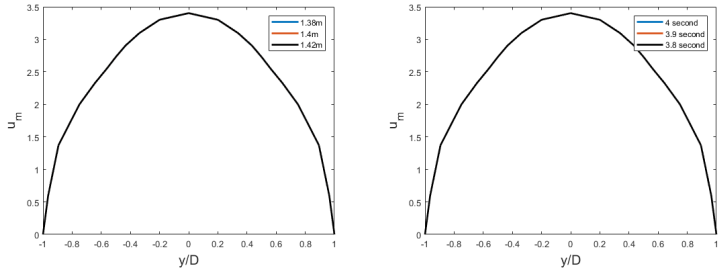

Figure 39: Mean Velocity Profiles of $Re = 1500$. From left to right: spatial and time convergence

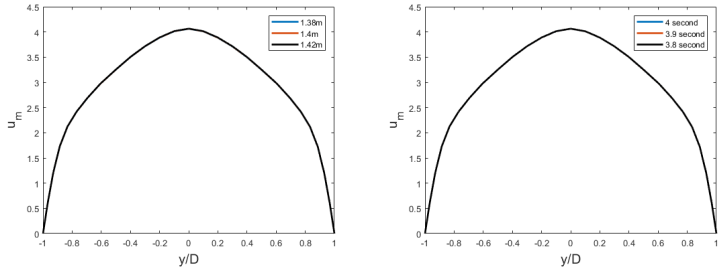

Figure 40: Mean Velocity Profiles of $Re = 1800$. From left to right: spatial and time convergence

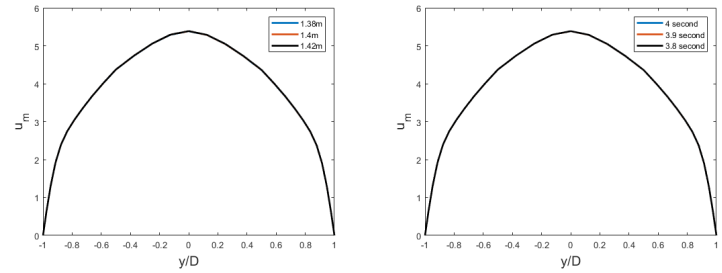

Figure 41: Mean Velocity Profiles of $Re = 2400$. From left to right: spatial and time convergence

Appendix E Velocity fluctuations plots for $Re = 1500, 1800$ and 2400

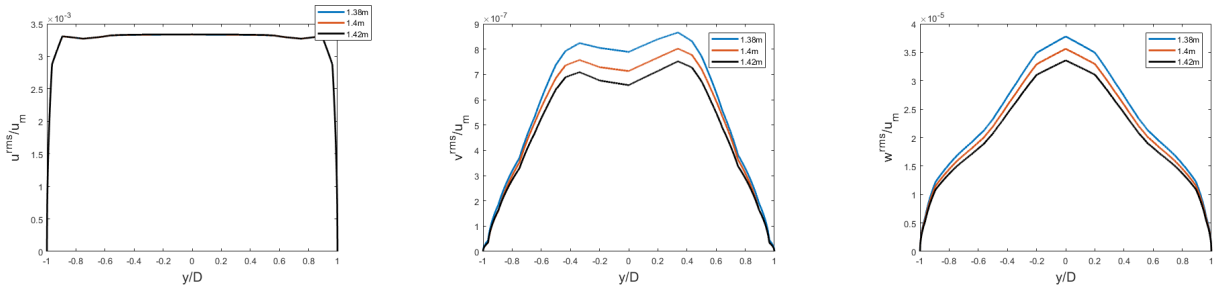

(a) $\frac{u^{rms}}{u_m}$ (b) $\frac{v^{rms}}{u_m}$ (c) $\frac{w^{rms}}{u_m}$

Figure 42: Profiles of fluctuating velocity of $Re = 1500$ for spatial convergence

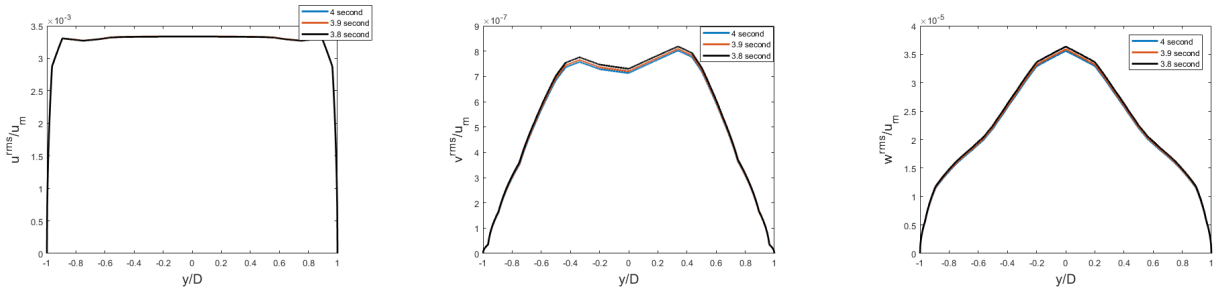

(a) $\frac{u^{rms}}{u_m}$ (b) $\frac{v^{rms}}{u_m}$ (c) $\frac{w^{rms}}{u_m}$

Figure 43: Profiles of fluctuating velocity of $Re = 1500$ for temporal convergence

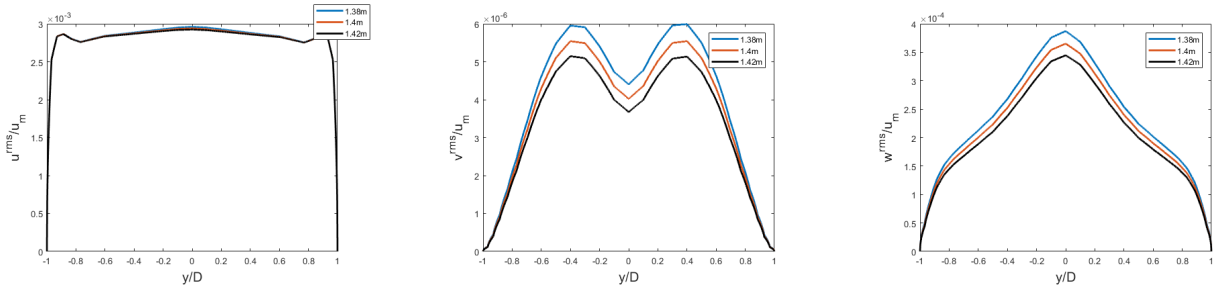

(a) $\frac{u^{rms}}{u_m}$ (b) $\frac{v^{rms}}{u_m}$ (c) $\frac{w^{rms}}{u_m}$

Figure 44: Profiles of fluctuating velocity of $Re = 1800$ for spatial convergence

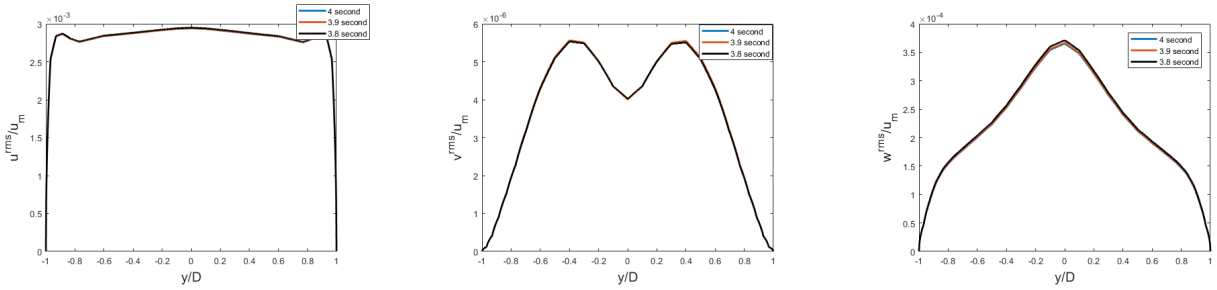

(a) $\frac{u^{rms}}{u_m}$ (b) $\frac{v^{rms}}{u_m}$ (c) $\frac{w^{rms}}{u_m}$

Figure 45: Profiles of fluctuating velocity of $Re = 1800$ for temporal convergence

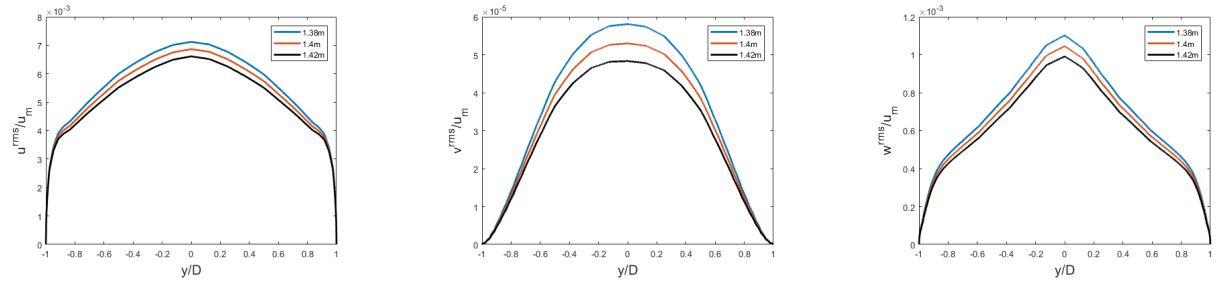

(a) $\frac{u^{rms}}{u_m}$ (b) $\frac{v^{rms}}{u_m}$ (c) $\frac{w^{rms}}{u_m}$

Figure 46: Profiles of fluctuating velocity of $Re = 2400$ for spatial convergence

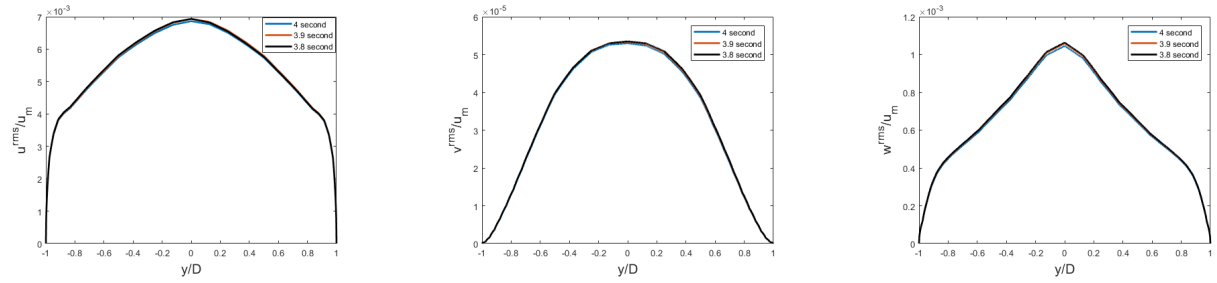

(a) $\frac{u^{rms}}{u_m}$ (b) $\frac{v^{rms}}{u_m}$ (c) $\frac{w^{rms}}{u_m}$

Figure 47: Profiles of fluctuating velocity of $Re = 2400$ for temporal convergence

Appendix F Turbulent shear stress plots for $Re = 1500, 1800$ and 2400

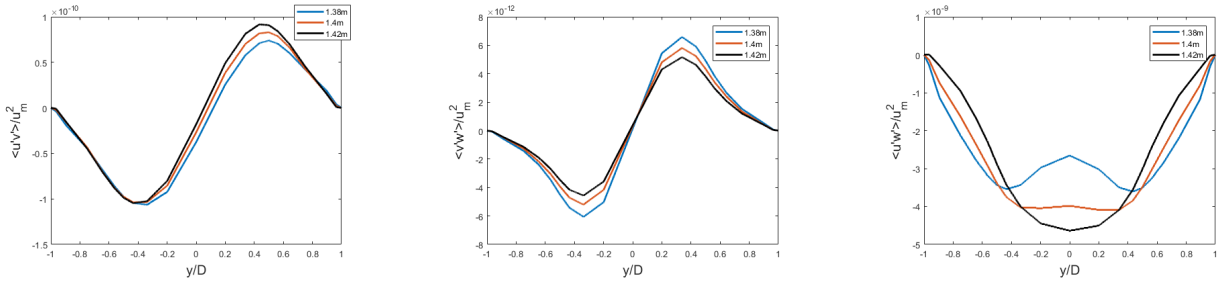

(a) $\frac{<u'v'>}{u_m^2}$ (b) $\frac{<v'w'>}{u_m^2}$ (c) $\frac{<u'w'>}{u_m^2}$

Figure 48: Turbulent shear stress components of $Re = 1500$ for spatial convergence

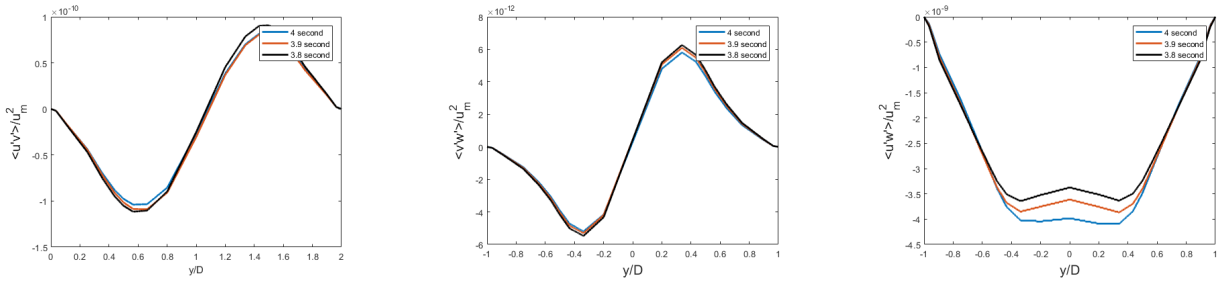

(a) $\frac{<u'v'>}{u_m^2}$ (b) $\frac{<v'w'>}{u_m^2}$ (c) $\frac{<u'w'>}{u_m^2}$

Figure 49: Turbulent shear stress components of $Re = 1500$ for temporal convergence

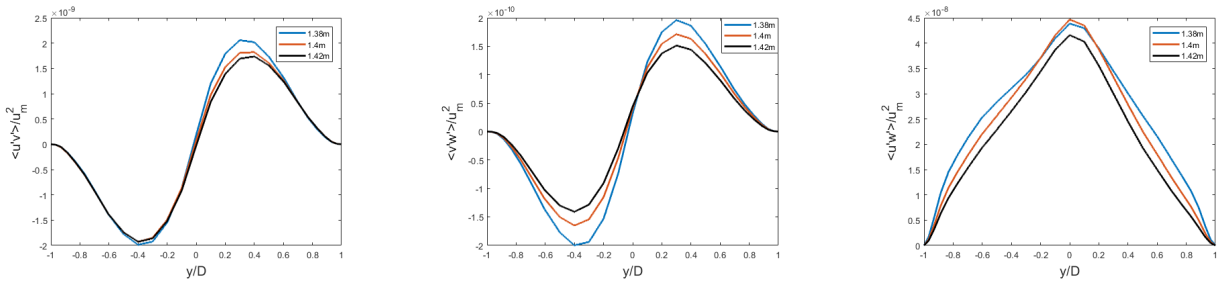

(a) $\frac{<u'v'>}{u_m^2}$ (b) $\frac{<v'w'>}{u_m^2}$ (c) $\frac{<u'w'>}{u_m^2}$

Figure 50: Turbulent shear stress components of $Re = 1800$ for spatial convergence

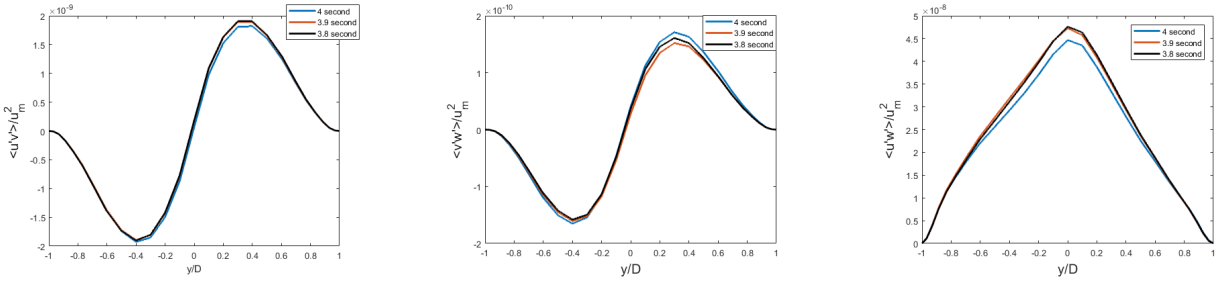

(a) $\frac{<u'v'>}{u_m^2}$ (b) $\frac{<v'w'>}{u_m^2}$ (c) $\frac{<u'w'>}{u_m^2}$

Figure 51: Turbulent shear stress components of $Re = 1800$ for temporal convergence

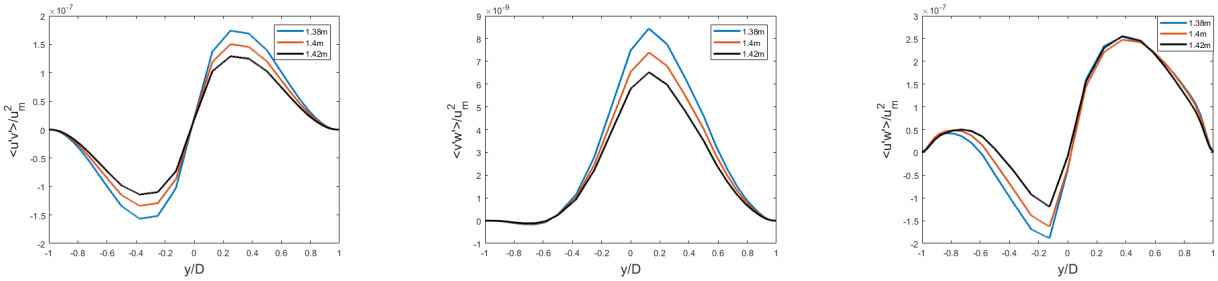

(a) $\frac{<u'v'>}{u_m^2}$ (b) $\frac{<v'w'>}{u_m^2}$ (c) $\frac{<u'w'>}{u_m^2}$

Figure 52: Turbulent shear stress components of $Re = 2400$ for spatial convergence

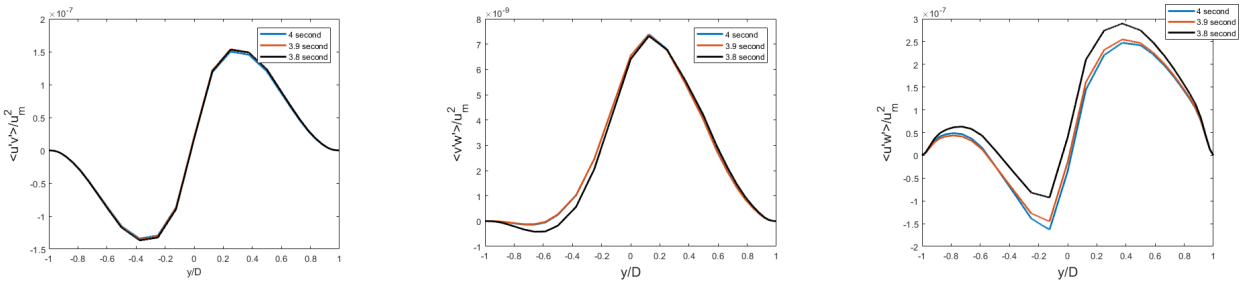

(a) $\frac{<u'v'>}{u_m^2}$ (b) $\frac{<v'w'>}{u_m^2}$ (c) $\frac{<u'w'>}{u_m^2}$

Figure 53: Turbulent shear stress components of $Re = 2400$ for temporal convergence

Appendix G Streamlines and Profiles

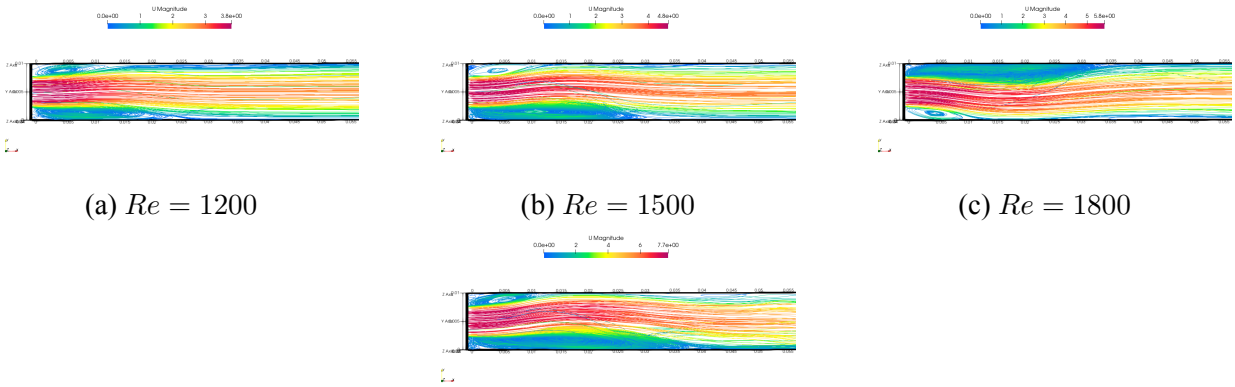

(a) $Re = 1200$ (b) $Re = 1500$ (c) $Re = 1800$

(d) $Re = 2400$

Figure 54: Recirculation region near inlet of channel at t=4s

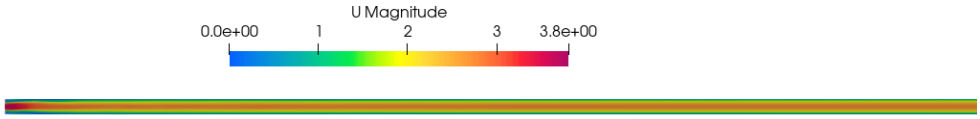

(a) $Re = 1200$

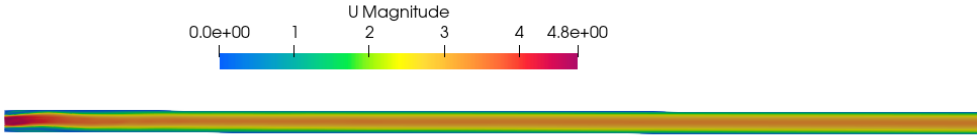

(b) $Re = 1500$

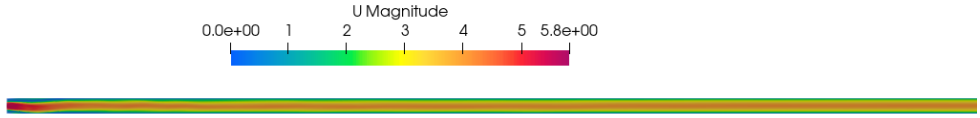

(c) $Re = 1800$

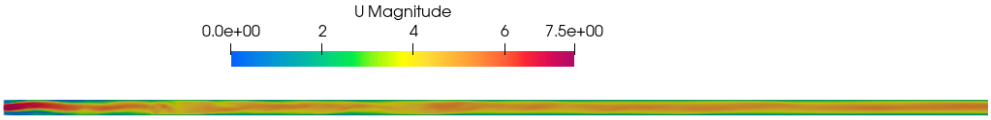

(d) $Re = 2400$

Figure 55: Velocity contour at xy cross-section of the channel at t=4s

Appendix H Turbulent Kinetic Energy at yz cross-sectional plane

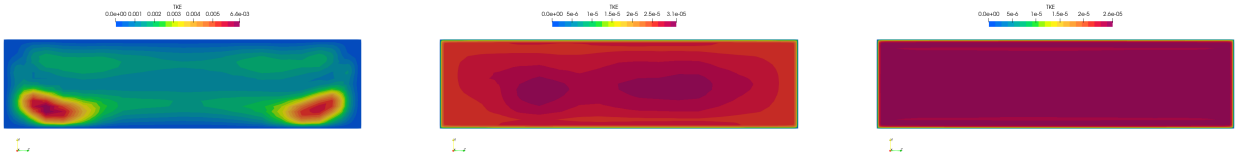

(a) x=0.1m (b) x=0.75m (c) x=1.4m

Figure 56: Turbulent Kinetic Energy profiles for $Re = 1500$

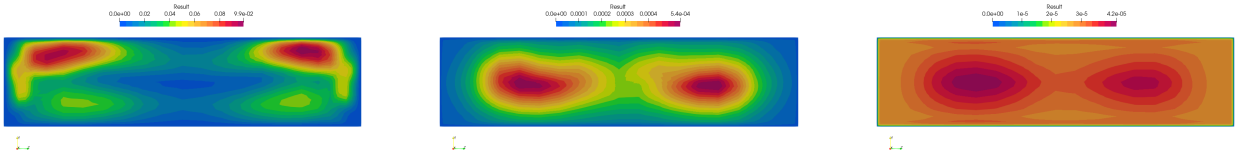

(a) x=0.1m (b) x=0.75m (c) x=1.4m

Figure 57: Turbulent Kinetic Energy profiles for $Re = 1800$

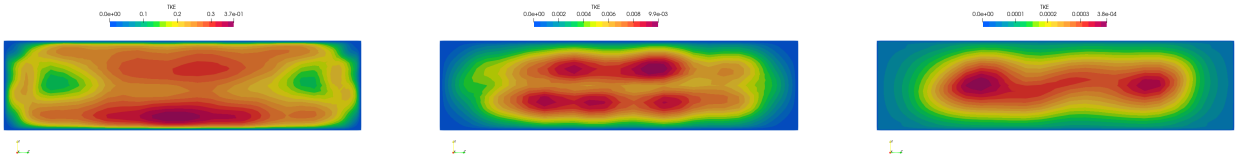

(a) x=0.1m (b) x=0.75m (c) x=1.4m

Figure 58: Turbulent Kinetic Energy profiles for $Re = 2400$

Appendix I Animation using Q-criterion of vortical structures

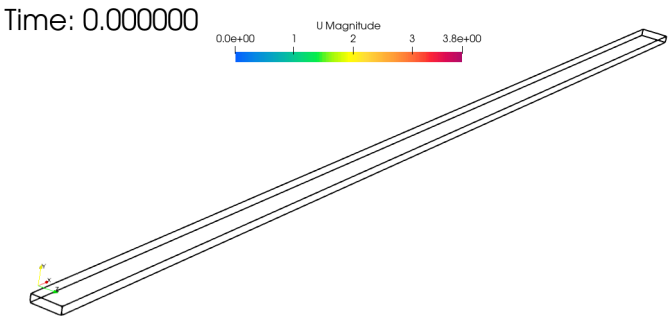

$Re = 1200$

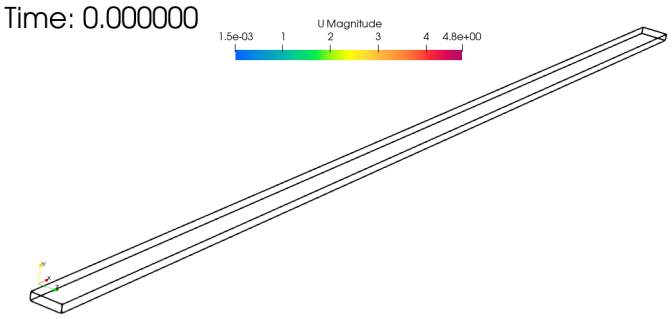

$Re = 1500$

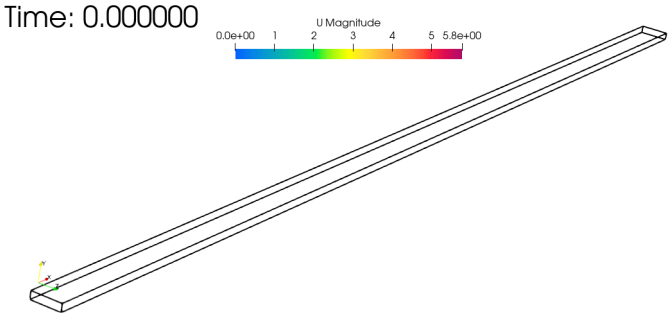

$Re = 1800$

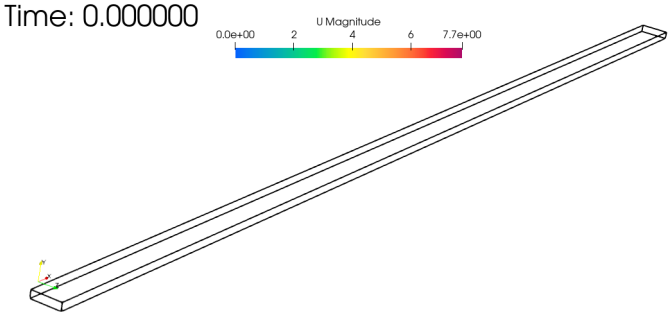

$Re = 2400$

Appendix J Python Code to plot power spectrum from velocity signal

```
fileName="Solution.dat"
fileObj=open(fileName)
linesBeforeData=0
for line in fileObj:
    line=line.strip()
    linesBeforeData +=1
    if line=="#Time":break

import numpy as np
import matplotlib.pyplot as plt

data=np.loadtxt(fileName,skiprows=linesBeforeData,unpack=True)

time=data[1]
Signal= data[2]


xin = Signal
Ta = time[2] - time[1]

N = len(xin)

   # sampling frequency
fa = 1 / Ta

    # fft
Xinn = np.fft.fft(xin)
#Xin=np.abs(Xinn)
Xn = 1 / N * Xinn
df = fa / N
f=np.arange(0,fa/2+df,df)

length = len(f)


Xs=np.transpose(Xn[0])


Xs = 2 * Xn[0:length]
```

```
a=np.power(f,-5/3)

y= 5*a;

plt.figure(1)
plt.loglog(f,np.abs(Xs),f,y)
plt.xlabel('Frequency(Hz)')
plt.ylabel('Power/Amplitude')
```

References

Cohen, J. and Wygnanski, I. (1987). The evolution of instabilities in the axisymmetric jet. part 1. the linear growth of disturbances near the nozzle. *Journal of Fluid Mechanics*, 176:191–219.

Gohil, T. B., Saha, A. K., and Muralidhar, K. (2012). Numerical study of instability mechanisms in a circular jet at low reynolds numbers. *Computers and Fluids*, 64:1–18.

Gohil, T. B., Saha, A. K., and Muralidhar, K. (2013). Direct numerical simulation of forced circular jets: Effect of varicose perturbation. *International Journal of Heat and Fluid Flow*, 44:524–541.

Hanks, R. W. and Ruo, H. C. (1966). Laminar-turbulent transition in ducts of rectangular cross section. *Industrial & Engineering Chemistry Fundamentals*, 5(4):558–561.

Klein, M., Sadiki, A., and Janicka, J. (2003). Investigation of the influence of the reynolds number on a plane jet using direct numerical simulation. *International Journal of Heat and Fluid Flow*, 24(6):785–794.

Lee, M. and Moser, R. D. (2015). Direct numerical simulation of turbulent channel flow up to $Re_\tau \approx 5200$. *Journal of Fluid Mechanics*, 774:395–415.

Lien, K., Monty, J., Chong, M., and Ooi, A. (2004). The entrance length for fully developed turbulent channel flow.

O'neill, P., Soria, J., and Honnery, D. (2004). The stability of low reynolds number round jets. *Experiments in Fluids*, 36:473–483.

OpenFoamWiki (v2006). Pimplefoam algorithm. `https://openfoamwiki.net/index.php/OpenFOAM_guide/The_PIMPLE_algorithm_in_OpenFOAM`.

Payri, R., López, J. J., Martí-Aldaraví, P., and Giraldo, J. S. (2016). Effect of turbulent model closure and type of inlet boundary condition on a large eddy simulation of a non-reacting jet with co-flow stream. *International Journal of Heat and Fluid Flow*, 61:545–552.

Pope, S. B. (2011). *Turbulent flows*. Cambridge Univ. Press, Cambridge.

Theofilis, V., Duck, P., and Owen, J. (2004). Viscous linear stability analysis of rectangular duct and cavity flows. *Journal of Fluid Mechanics*, 505.

xu, H., Khalid, M., and Pollard, A. (2003). Large eddy simulation of turbulent flow in confined square coaxial jet. *International Journal of Computational Fluid Dynamics*, 17.